TRANSONIC CFD APPLICATIONS AT BOEING

E. N. Tinoco
Computational Fluid Dynamics Laboratory
Boeing Commercial Airplane Company
Seattle, Washington

SUMMARY

The use of computational methods for three-dimensional transonic flow design and analysis at the Boeing Company is presented. A range of computational "tools" consisting of "production" tools for everyday use by project engineers, "expert user" tools for special applications by computational researchers, and a new "emerging" tool which may see considerable use in the near future are described. These methods include full potential and Euler solvers, some coupled to three-dimensional boundary layer analysis methods, for transonic flow analysis about nacelle, wing-body, wing-body-strut-nacelle, and complete airplane configurations. As the examples presented show, such a toolbox of codes is necessary for the variety of applications typical of an industrial environment. Such a toolbox of codes makes possible aerodynamic advances not previously achievable in a timely manner, if at all.

INTRODUCTION

Computational Fluid Dynamics (CFD) is playing an ever increasing role in the design of air vehicles. CFD has joined the wind tunnel and flight test as a principal technology for aerodynamic design. When the next new Boeing airplane flies, whether an all new design, or a derivative of an existing production aircraft, CFD will play a role in its design. The proper and timely use of CFD will result in a superior product with reduced risk and lower cost. However, note success does not come automatically with CFD, the keys to success are the "proper and timely use."

CFD today covers a wide range of capabilities in terms of computational flow physics and geometrical complexity. Figure 1 illustrates the boundary in terms of the complexity of flow physics and configuration geometry that encompass what we believe is practical in industry. We realize that this boundary is continuously being challenged by researchers here and abroad.

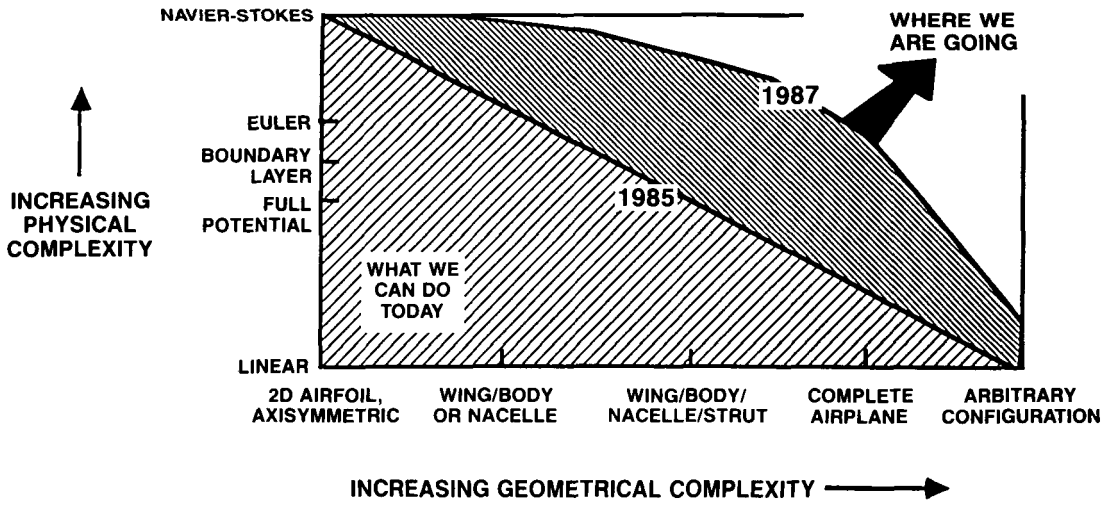

Figure 1. Status of CFD for Design Application.

The value of CFD in industry is in its application. CFD is used to lend understanding to the flow phenomena about a given geometry and to aid in the design of a piece of hardware, whether it be an all new wing, or a minor modification to an existing configuration. To be useful the computational method must faithfully represent the dominant flow physics, adequately represent the required geometrical complexity, be capable of providing solutions in a timely manner, and be affordable. This is a tall, and as yet unfilled, order by any single method. The approach at Boeing has been to assemble a toolbox with a collection of CFD tools that meets the above requirements to varying degrees. In this toolbox are "production" tools that are in wide use throughout the company by a variety of CFD users. These are well documented codes that have been specialized to a certain extent, and can be run by the nonexpert CFD users. There are "expert user" tools, which may have more general and advanced capabilities than the "production" codes, but are not as well developed, and may require special skill to run successfully. There are also "emerging" tools. New technologies under development, offer new capabilities, which may become "production" tools in the near future.

No CFD toolbox is complete without geometry and graphics tools. Geometry tools are essential for the preparation of the inputs to the various CFD codes. Three-dimensional graphics running on suitable workstations allow the inspection of surface and field grids prior to execution, and provide the keys to understanding the frequently massive output from a typical transonic CFD solution. The "timeliness" of CFD is very heavily tied into the quality of the geometry and graphics tools available. The primary tool fitting this need at Boeing is the interactive, three-dimensional geometry system known as the Aero Grid and Paneling System (AGPS), Reference 1. AGPS provides an efficient means of defining any three-dimensional surface or aircraft component. These surfaces can be combined to represent a complete aircraft configuration. AGPS has built-in and user-programmable features for extracting geometric data in the proper form for use by CFD codes. Paneling, surface grid generation, and grid distribution at block boundaries for input to three-dimensional grid generation codes are all possible. AGPS can also display CFD results in the form of three-dimensional objects with color representing the value of some flow property. Several other geometry and graphics codes are also essential parts of the toolbox.

Table 1. Transonic CFD Toolbox

PRODUCTION CODES	FORMULATION	GEOMETRY CAPABILITY
A502/PANAIR	Linear Potential	General Geometry
A488	Conservative Full Potential with Coupled 3-D Boundary Layer - Analysis	Wing-Body, Wing-Body-Strut-Nacelle
A555	Conservative Full Potential with 3-D Boundary Layer - Design	Wing-Body Wing-Body-Strut-Nacelle
A588	3-D Euler with Coupled 3-D Boundary Layer	Isolated Turbofan Nacelle Isolated Turbofan Nacelle-Strut
P318	Axisymmetric Full Potential with Boundary Layer	Isolated Axisymmetric Nacelle
P467	Full Potential with 3-D Boundary Layer	Axisymmetric Nacelle
P582	Full potential	General Geometry
WBPPW/BOPPE	Extended Transonic Small Disturbance with Coupled Boundary Layer	Wing-Body-Strut-Nacelle-Winglet
EXPERT USER CODES		
	Euler	Wing-Body-Tail Wing-Body-Tail-Aft Propfan UDF Nacelle-Strut Turbofan Nacelle
	Euler with Coupled 3-D Boundary Layer	Wing-Body-Tail Wing-Body-Strut-Aft Propfan Wing-Body-Winglet
EMERGING CODE		
TRANAIR	Full Potential	General Geometry

This paper will go on to describe the various CFD tools in use at Boeing, and in this manner will illustrate how transonic CFD methods are used. The perspective presented is mainly from the view of the Boeing Commercial Airplane Company. However, these methods are available, and are used by other members of The Boeing Company. The focus of this paper is on transonic CFD methods for three-dimensional flows. Table 1 lists some of the common CFD tools in use at Boeing today.

SYMBOLS

A = streamtube area

b = wingspan

C_d = section drag coefficient

C_D = drag coefficient

C_ℓ = section lift coefficient

C_L = lift coefficient

C_{nf} = normal force coefficient

C_p = pressure coefficient

c = wing chord

FNPR = fan nozzle pressure ratio

M = Mach number

T_c = Thrust coefficient

x = streamwise coordinate

y = lateral coordinate

z = vertical coordinate

α = angle of attack

β = side slip angle

δ^* = boundary layer displacement thickness

η = span fraction

Subscripts

H = inlet highlite

I = inlet

∞ = freestream

T = total

PRODUCTION TOOLS

Production tools or codes are characterized by the following: they are used outside the research organization that created them; their documentation is adequate enough to allow use by other than their creators; stable versions of these codes exist for use outside the research environment that are not undergoing constant change; sufficient validation of these codes has been demonstrated such that outside users are willing to invest the necessary effort to use them.

Two production codes that see the most use in Boeing are A502/PANAIR, a linear panel method, and A488, a full-potential solver with coupled boundary layer analysis for wing-body and wing-body-strut-nacelle configurations. These two codes are accessed over 2,000 times a year each. Although A502/PANAIR (refs 2 and 3) is not a true transonic method, its ability to model complex detailed geometry, makes it the only currently usable tool in some instances. In the design of the Navy E-6A wingtip pod arrangement, shown in Figure 2, only A502/PANAIR could handle the complex geometry at the time. It was used in the design process to shape the pods and struts to minimize supercritical flow at cruise conditions. The resulting design was committed to manufacture and first saw real air when it flew on the aircraft. Only the emerging full-potential TRANAIR code promises the ability to deal with fine geometric details such as tip pods, stores, or missiles, etc. in a supercritical flow environment. TRANAIR will be discussed in more detail later in this paper.

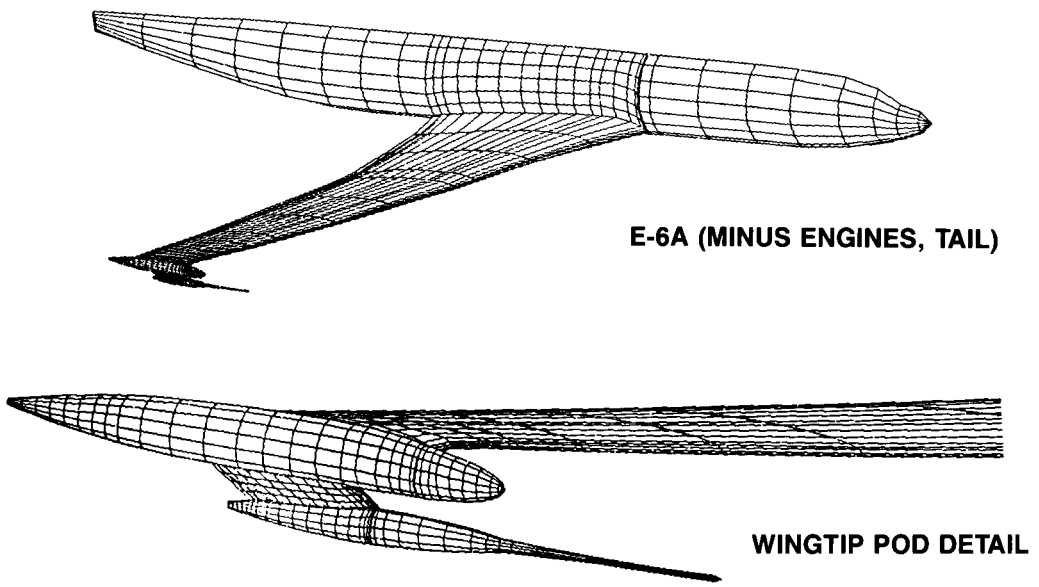

Figure 2. E-6A Wingtip Pod—A CFD Design.

For most analyses of wing-body, or wing-body-strut-nacelle configurations at Boeing, A488 is the code of choice. A488 couples a full-potential inviscid flow solver with a three-dimensional boundary layer solution for the wing. It has been undergoing continuous development and refinement for the last 10 years. The method was first demonstrated in 1978 (ref 4), and has evolved into a highly sophisticated analysis tool that will rival any Navier-Stokes solver for accuracy at a small fraction of the cost for analysis of attached flows. A488 has evolved into a system of some 50 programs tied together with job-control language. Use of the system requires user access to numerical lofts of the wing (in either of two commonly used geometry systems at Boeing), body, nacelle, and strut, or files consisting of normal station cuts for the body and nacelle, and waterline cuts for the strut. An input file is prepared containing flow condition information, i.e., Mach, angle of attack, Reynolds number, etc.; transition strip location as a function of span fraction, etc.; and file names of the various geometric components. An online program is executed that generates all the job-control logic and submits the problem for execution on a CRAY X-MP. The grid generation, and cycling between the inviscid and viscous solvers automatically proceeds for the prescribed number of iterations, as illustrated in Figure 3.

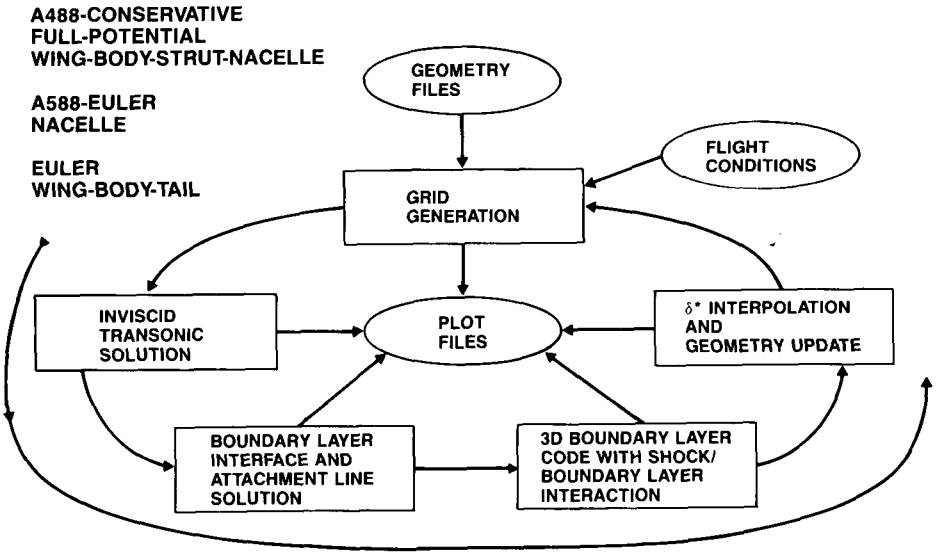

Figure 3. Integrated Transonic/Viscous Analysis System.

A flexible and efficient elliptic grid generation method (refs 5 and 6) is used to generate a surface-fitted C-type grid. The grid distribution along the strut-nacelle requires special consideration. For a general strut-nacelle installation, it is usually difficult to produce an exact surface-fitted grid with smooth and well distributed mesh spacing in the field. The approach taken here involves a simplification of the nacelle inlet geometry and a relaxation of the requirement that the grid lines lie along the corners formed by the nacelle-strut intersection and along the nacelle keel line, as illustrated in Figure 4. The tight clustering of grid lines close to the wing allows adequate grid resolution in the region between the wing lower surface and the nacelle. The exhaust plume is modeled as a solid surface. With the proper choice of the exhaust plume shape (ref 7), both power effects and core cowl shape effects can be simulated.

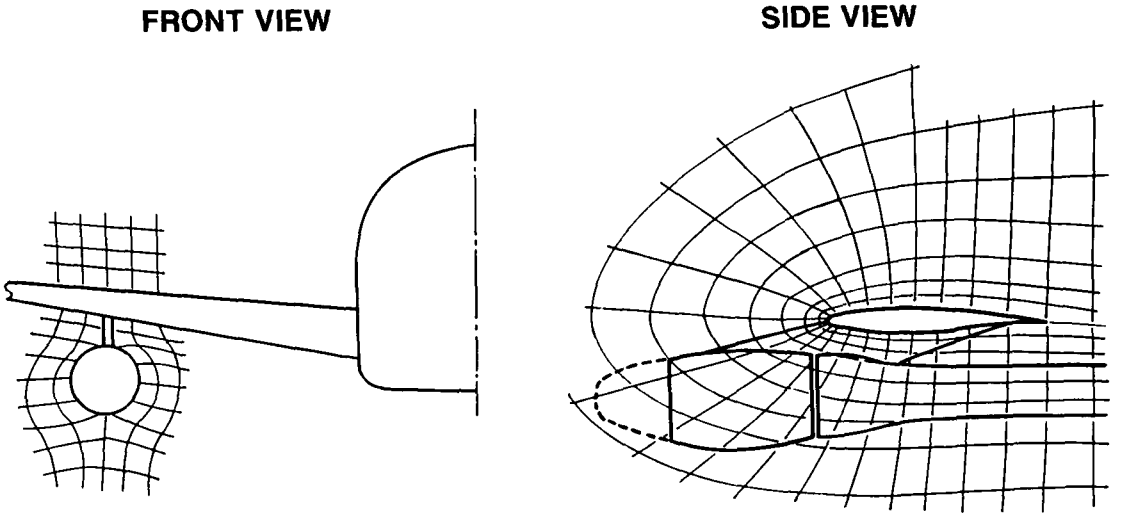

Figure 4. Grid Topology at Nacelle/Strut Station.

The current inviscid solver is based on the full-potential, fully conservative Jameson-Caughey finite volume algorithm, FLO28 (ref 8). Enhancements added to the method include: a convergence acceleration method using an extrapolation technique (ref 9), and GMRES (ref 10); second-order accurate differencing for better shock resolution; and, improvements to the calculation of surface pressures and the Kutta condition.

The boundary layer calculations are based on the method of McLean (ref 11). This is a three-dimensional finite difference formulation for both laminar and turbulent boundary layers. In addition, a semiempirical shock-boundary layer interaction model (ref 12) has been added. Here, the treatment of the effects of a shock on the boundary layer is improved by replacing the boundary layer equations in the shock zone with a set of empirical jump conditions for the changes in the boundary layer quantities through the shock. The boundary layer equations are still used upstream and downstream of the shock zone. The determination of the shock zone is based on the behavior of the shock-perpendicular Mach number. The method also includes an attachment line solution at the wing leading edge which is used to determine the starting conditions for the upper and lower surface boundary layer solution.

The interaction between the boundary layer and the inviscid flow is calculated by a classical direct-iteration scheme. In each cycle of the iterative procedure, the viscous flow is computed in the direct mode (i.e., given the velocity components from the inviscid outer solution calculate the boundary layer and output the displacement thickness), and a weighted average of the new and old displacement thickness is used to modify the surface shape for the next cycle. The field grid for the inviscid solver is automatically updated with each displacement thickness change.

A488 results have been compared with experimental data for a variety of vehicles. Figure 5 shows a comparison of A488 results with wing pressure distributions measured in flight on a 737-300. The computational model consisted of the wing, body, strut, and nacelle. The wing definition included the estimated aeroelastic twist for the condition flown. Although the character of the pressure distribution on the wing changes dramatically across the span, the computational results agree reasonably well with the measured data.

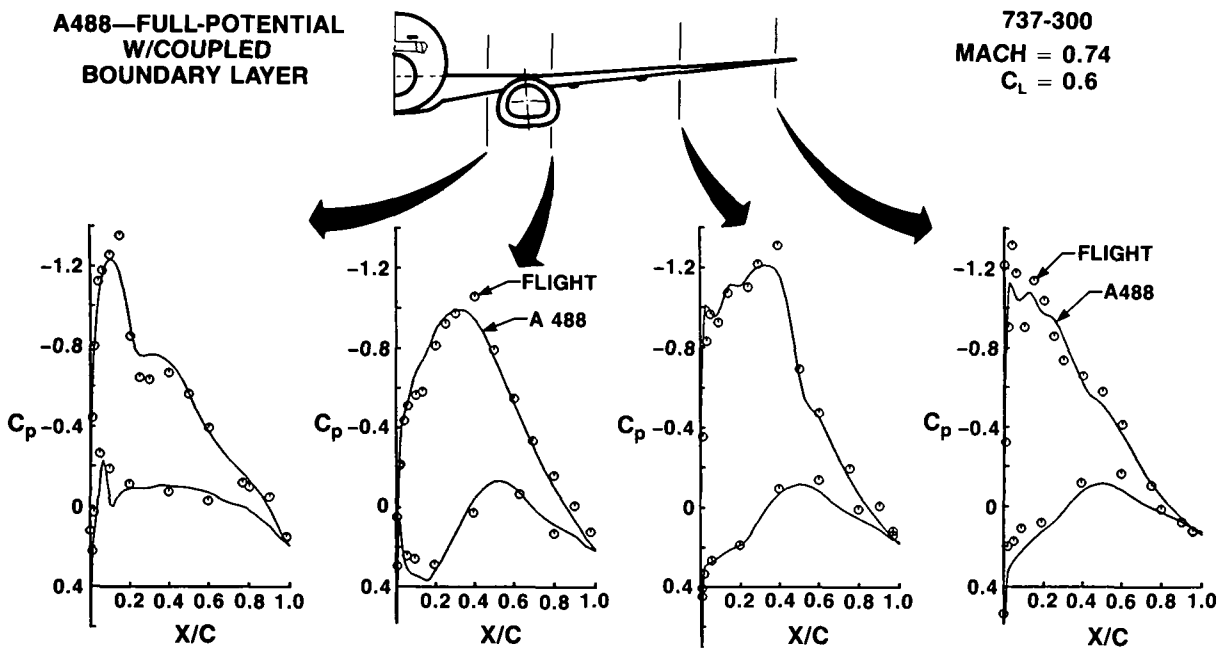

Figure 5. Comparison With Flight Pressure Distributions—737-300.

Figure 6 presents a comparison of spanwise distribution of section lift with wind tunnel data for an early developmental 757-200 wing-body-strut-nacelle configuration. This comparison illustrates the importance of accounting for the aeroelastic deflections that occur in the wind tunnel. The wind tunnel model was a full model with a steel wing and was tested in an atmospheric tunnel. At the dynamic pressure for Mach 0.80 and at the cruise lift, the estimated additional wing twist at the wingtip due to aeroelastics was 0.5 deg. Inclusion of the aeroelastic twist in the computational model definition was essential for good agreement with the experimental data.

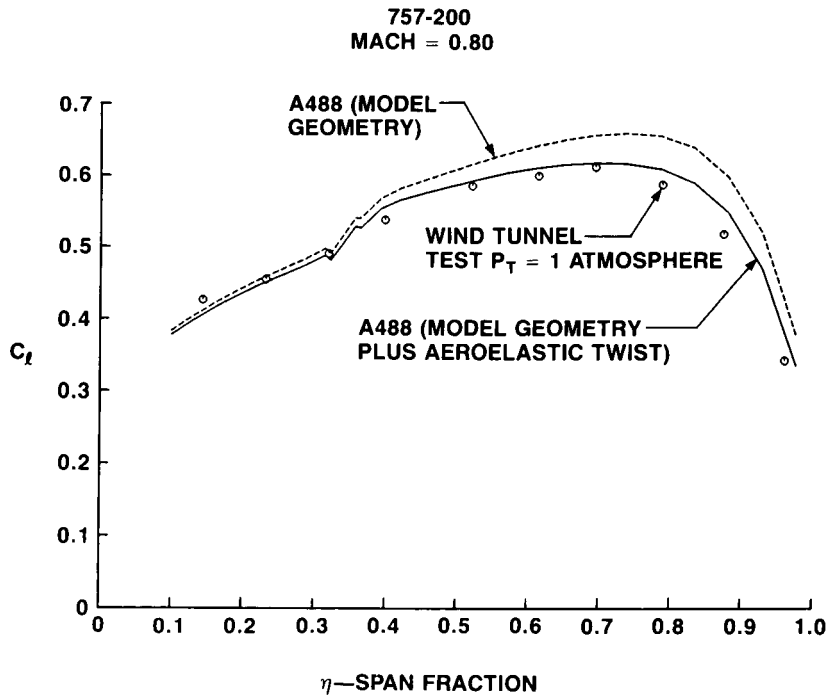

Figure 6. Comparison With Wind Tunnel Section Lift Distribution.

Figure 7 shows another comparison of A488 results with flight data. This time it shows a Grumman F-14 with the wing set at the 20-deg sweep position. These analyses were done in support of a variable sweep boundary layer transition flight experiment (ref 13). With the exception of the inner-most station, the computational results agree well with the measured data. The discrepancy at the most inboard station is believed to be due to the inability of the method, with its single block C-grid topology, to adequately represent the fuselage. The surface grid used for the analysis is shown in Figure 8. The general cross-section of the fuselage is represented but the engine inlet has been gridded over. This example illustrates the need for methods capable of handling more general and complex geometries.

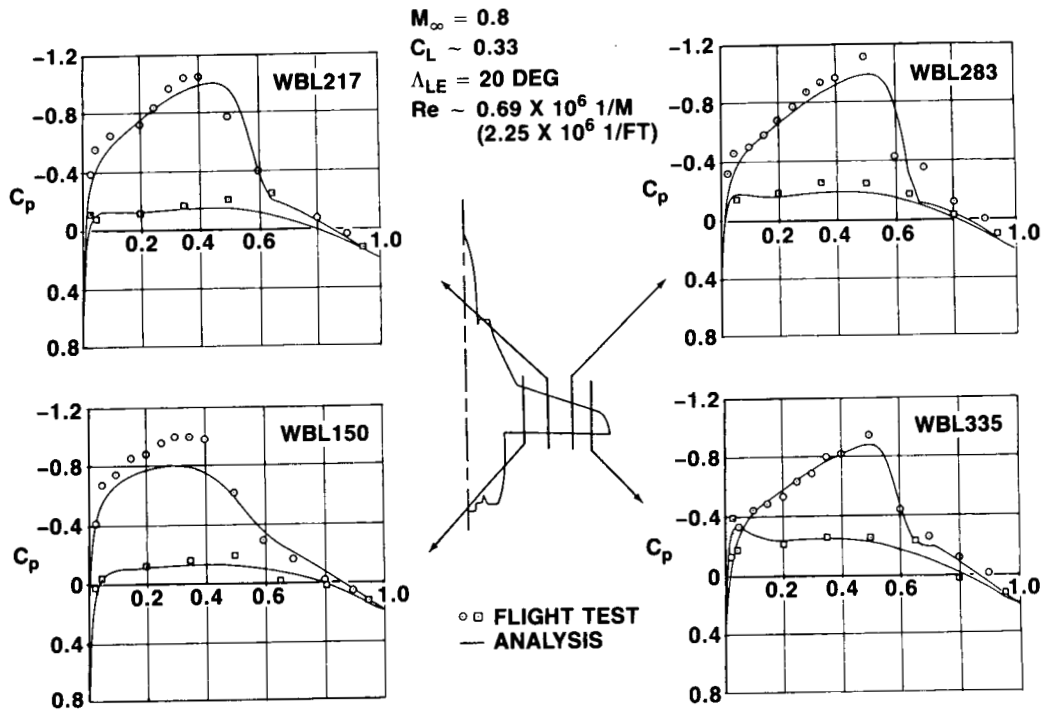

Figure 7. Comparison With Flight Pressure Distributions—F-14.

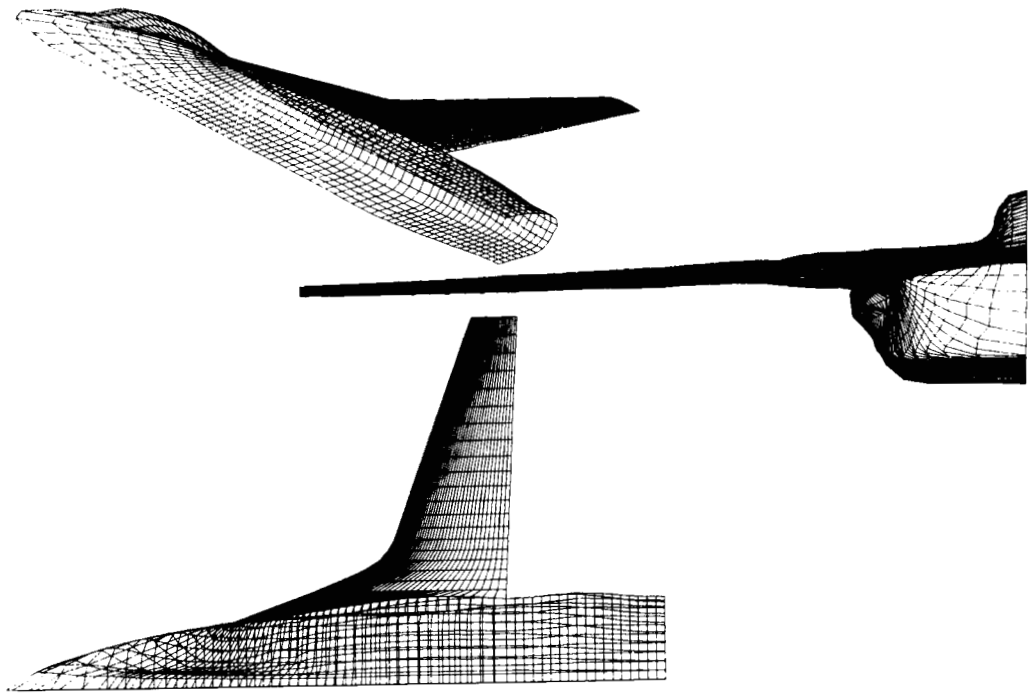

Figure 8. Surface Grid for F-14 in A488 Code.

In the solution process, detailed boundary layer characteristics are calculated. Using analyses at full-scale Reynolds number as a guide, trip strip patterns can be designed for low Reynolds number testing which will best result in a displacement thickness at the shock or trailing edge comparable to the expected full-scale value. The spanwise distribution of skin friction and profile drag can also be derived from the boundary layer calculations. The profile drag is based on applying the Squire Young formula (ref 14), along the wing trailing edge. Only the streamwise components of the trailing-edge velocity profiles are used in this formulation. A comparison with measured profile drag is shown in Figure 9. The distribution and level of profile drag are in good agreement with the test data. The skin-friction drag distribution is shown for reference. The experimental profile drag was derived from a series of wake traverses along the wingspan. For subcritical flows, the wake total pressure deficit is due only to the profile drag. For supercritical cases wave drag also adds to the total pressure deficit. Figure 10 shows a comparison for wave drag and profile drag. Measured and calculated profile and wave drags agree reasonably well. Examination of the spanwise variation of wing drag components helps identify the critical wing design regions and allows for better wing design.

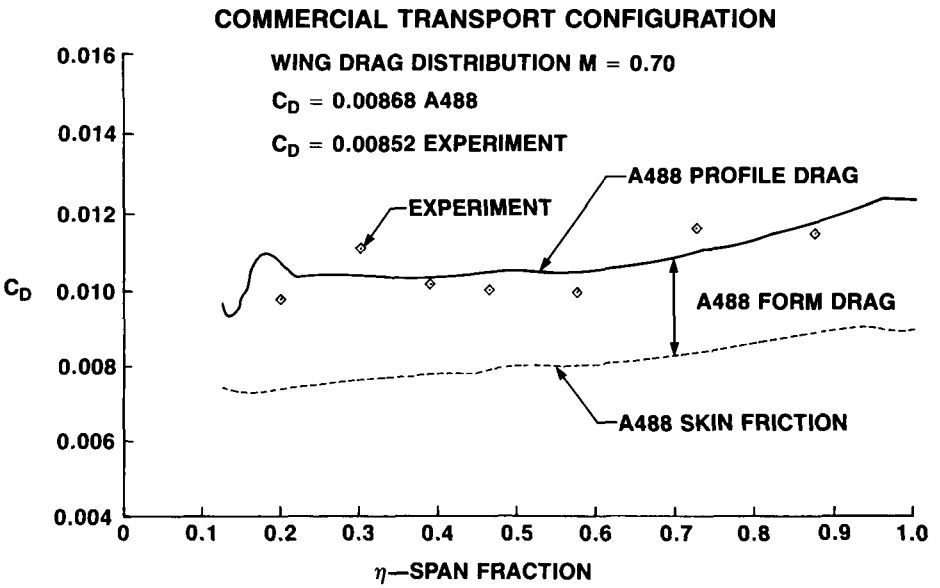

Figure 9. Wing Profile Drag Distribution—Test-Theory Comparison.

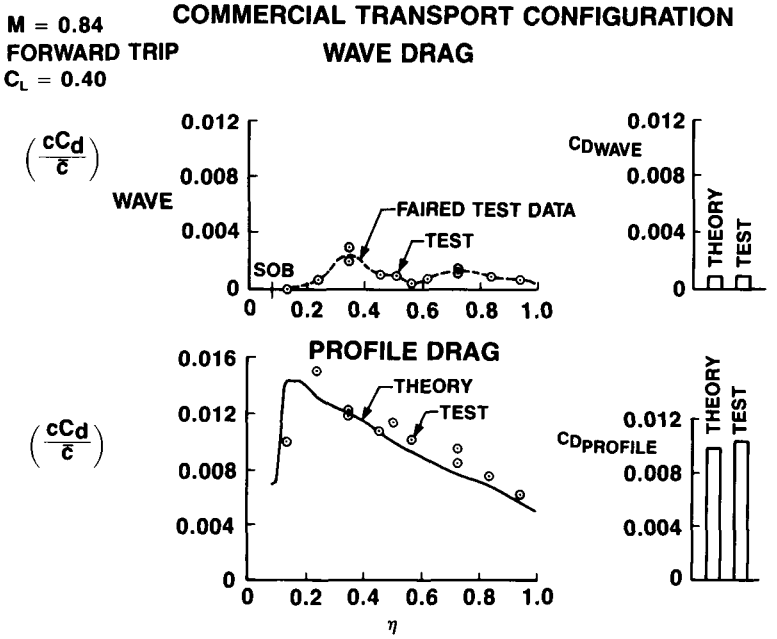

Figure 10. Spanwise Profile and Wave Drag Distributions, M = 0.84.

Accurate drag prediction is always of interest in industry. Although methods such as A488 can be used to develop drag polars (see Figure 11, for example), CFD has not yet matured to the level where it is capable of predicting complete airplane configuration drag to the accuracy needed for commercial transport development. The competitive nature of the commercial transport industry makes drag improvements of less than one percent airplane drag significant and worth seeking. CFD methods capable of reliably and accurately predicting drag values, even component drags, would be of great value to the aircraft designer. Methods like A488 may be able to do this for transport type wings with attached flow, but there is a lack of experimental data to adequately validate these methods. Adequate validation requires detailed test-theory comparisons at several combinations of Mach number, angle of attack, and Reynolds number. Not only are force data necessary for validation, detailed surface pressure data and wake measurements are also required.

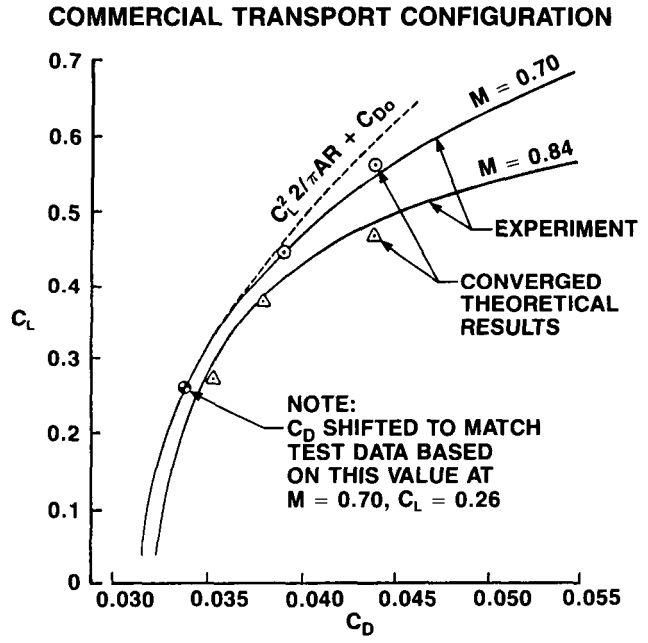

Figure 11. Comparison of Computational and Experimental Drag Polars.

The ability to adequately model the nacelle and strut is essential for many of our applications. The presence of the nacelle and strut can have a significant effect on surface pressures on the upper as well as the lower surface of the wing, as illustrated in Figure 12. We have had reasonable success in simulating engine installation details such as engine primary core cowl shape effects on wing lower surface pressure distributions (Fig 13), and engine power effects (Fig 14). Figure 13 shows the difference in wing lower surface pressure distribution that results when the engine primary core cowl is truncated to yield a desired inlet mass flow ratio in a wind tunnel flow through nacelle compared to what might be achieved by the actual engine geometry. Figure 14 shows the difference between the engine operating at cruise thrust or exhausting at "ram" fan nozzle pressure ratio, i.e., exhausting at free-stream Mach number. These effects are simulated by specification of the appropriate fan exhaust plume shape (ref 7).

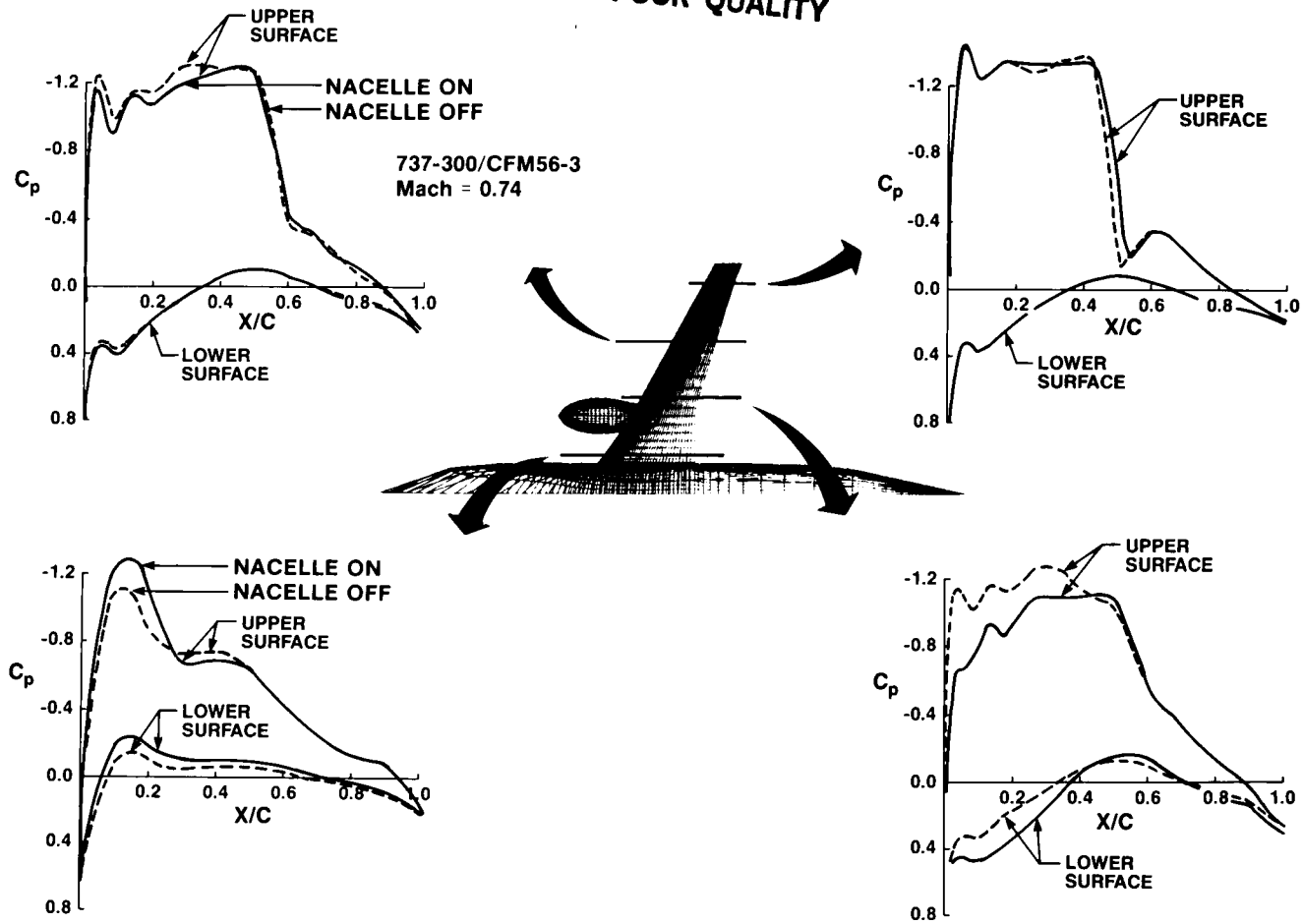

Figure 12. Influence of Nacelle on Wing Surface Pressures.

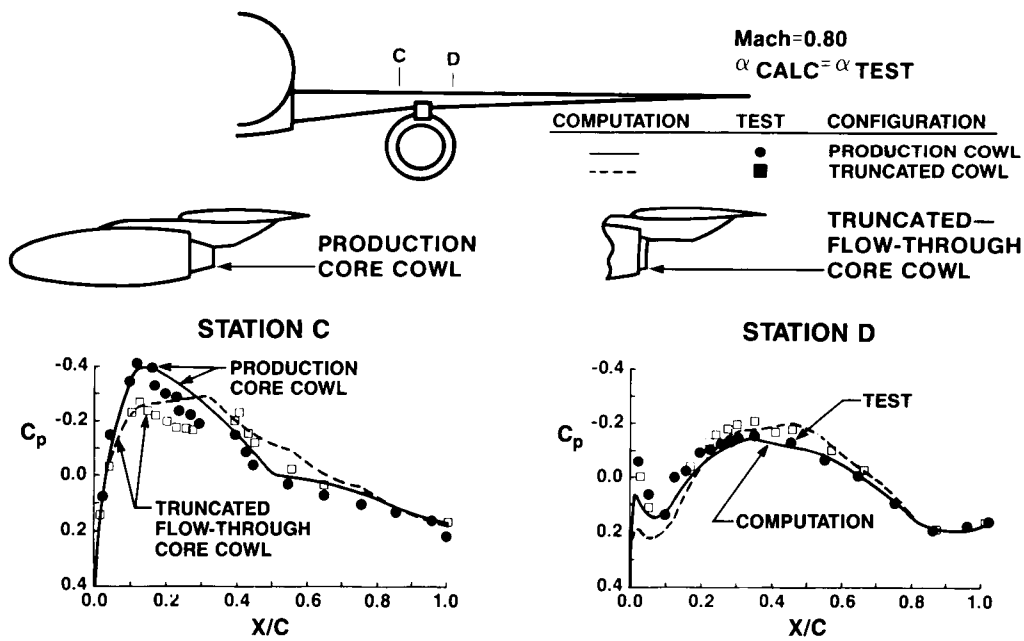

Figure 13. Core Cowl Geometry Effects.

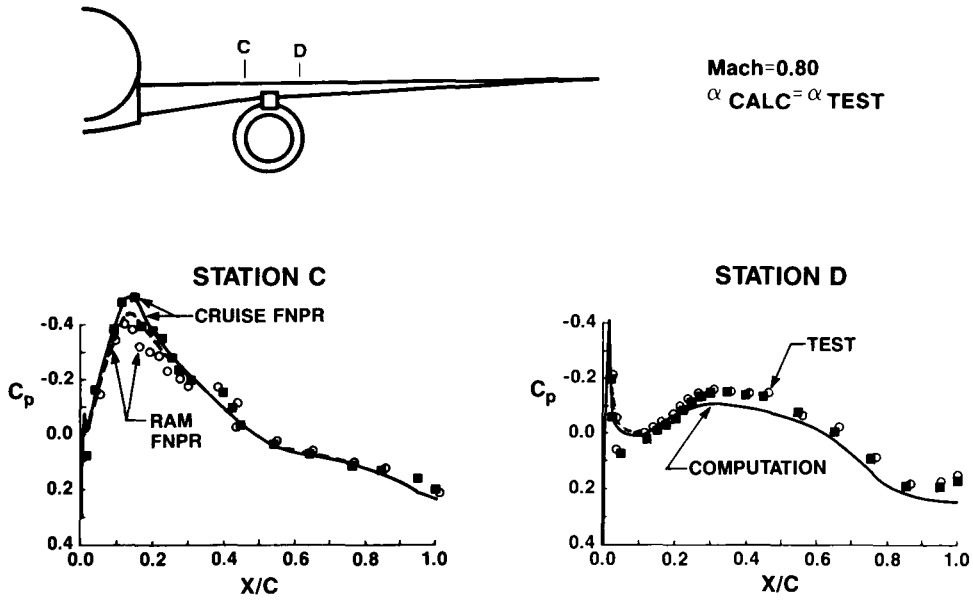

Figure 14. Power Effects on Wing Lower Surface.

Other applications of the A488 system have included evaluating out-of-contour fairings for a deeper landing gear-beam on the 737-400, wing modifications to several existing configurations, and aerodynamic analyses of several horizontal tails.

Originally developed in the early 1980s, but just recently elevated to production status is A555, an inverse design full-potential code with boundary layer effects. A555 is complementary to A488. Both use an enhanced version of FLO28 for their inviscid solver, and the same three-dimensional finite difference boundary layer code. The solutions are completely reversible, that is, one can take the pressure distribution from an A488 analysis, run it through A555 and recover the original A488 geometry. The use of A555 is illustrated in Figure 15. An initial seed geometry is first analyzed. If the resulting solution does not exhibit the desired

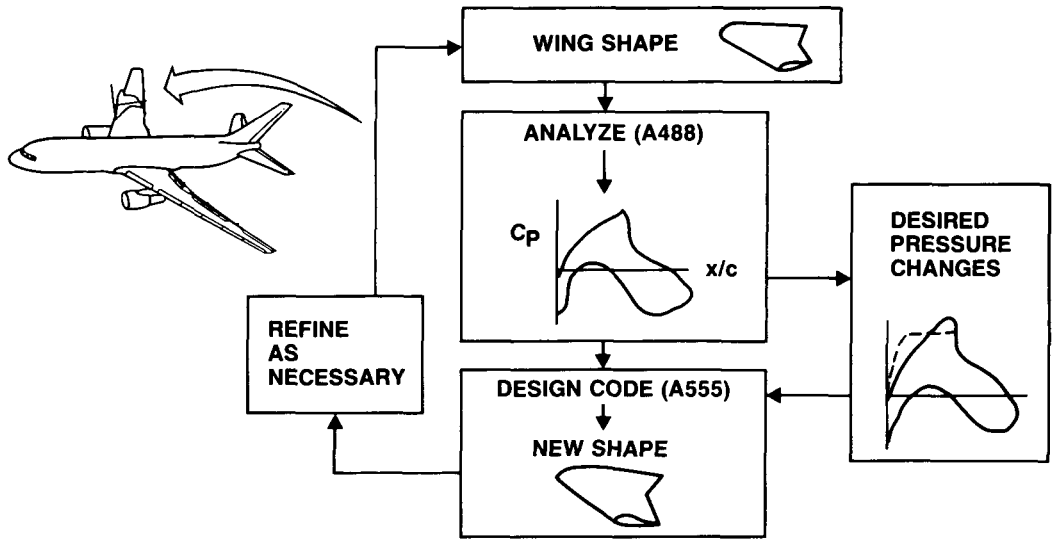

- Design and analysis with CFD
- Use wind tunnel to validate wing design

Figure 15. Wing Design Using CFD.

pressure distributions, the designer can specify a desired target pressure distribution. Several preprocessors are available to assist the designer in specifying distributions with the desired characteristics and proper smoothness. The inverse design code then produces a geometry which includes the boundary layer displacement thickness. The boundary layer solution supplies the displacement thickness to be removed, which after removal leaves the bare wing geometry. This resulting geometry is then modified as necessary to meet whatever manufacturing constraints might apply, and then reanalyzed. This cycle may be repeated several times until a wing design evolves having the desired pressure characteristics and meeting all the appropriate geometric constraints. The coordinated A488/A555 system has allowed wing designs to be developed in a timely manner that were not previously achievable.

Another transonic analysis code that is occasionally used at Boeing, because of its ability to model winglets in a simplified form, is the NASA WBPPW/Boppe code (ref 15). This code is based on an extended small disturbance transonic formulation, and features multiple-embedded grids. The code's use of linearized boundary conditions along with the multiple-embedded grids allows the user to avoid the complications of surface-fitted grid generation when analyzing configurations with winglets, pods, and pylons. A comparison of results from this code with experimental data acquired in the mid-1970s is shown in Figure 16. The ability to generate surface-fitted grids for wings with a full-chord winglet has recently been developed at Boeing allowing the use of full potential or Euler codes for winglet analysis.

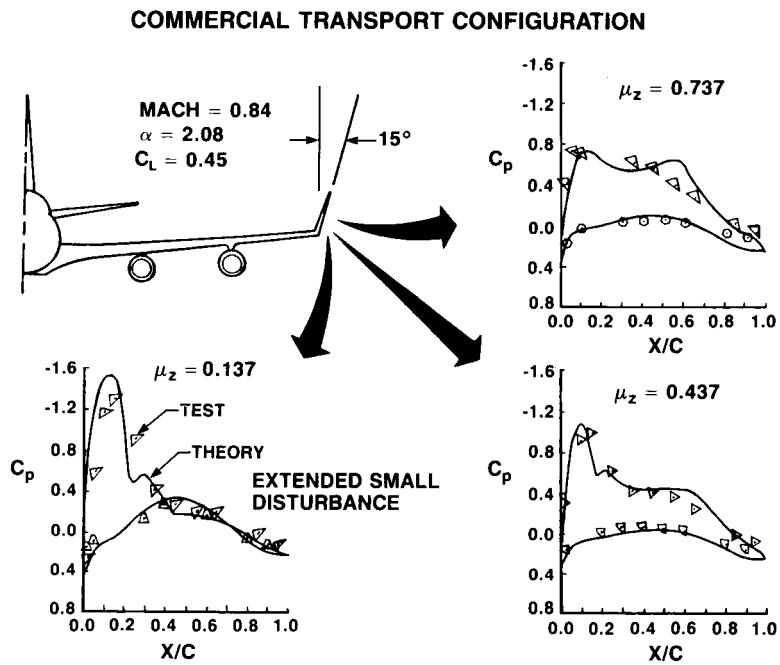

Figure 16. Winglet Pressure Distributions.

The grid topology of the A488 system does not allow detailed analysis of the flow on the nacelle, only its effects on the wing. For detailed analysis of a turbofan nacelle we use A588, a three-dimensional Euler solver coupled to the same three-dimensional finite difference boundary layer code as used in A488. The Euler nacelle code, developed for powered turbofan nacelle analysis (ref 16), is based on FLO57 (ref 17). It features a time-dependent solution of the Euler equations in conservative form. A C-type body-fitted computational grid, illustrated in Figure 17, is used. The code solves a two-stream problem comprised of external and fan flows. Core flow is treated either as a solid-body extension of the input geometry or the core cowl geometry is simply extended and terminated at a point. The nacelle mounting strut can also be included in the analysis. Boundary conditions can be specified on the inlet face to control the inlet mass flow. Total pressure, total temperature, and swirl can be specified on the exit plane in the fan exhaust duct to describe the exhaust conditions. The code is capable of analyzing both angle of attack and yaw conditions.

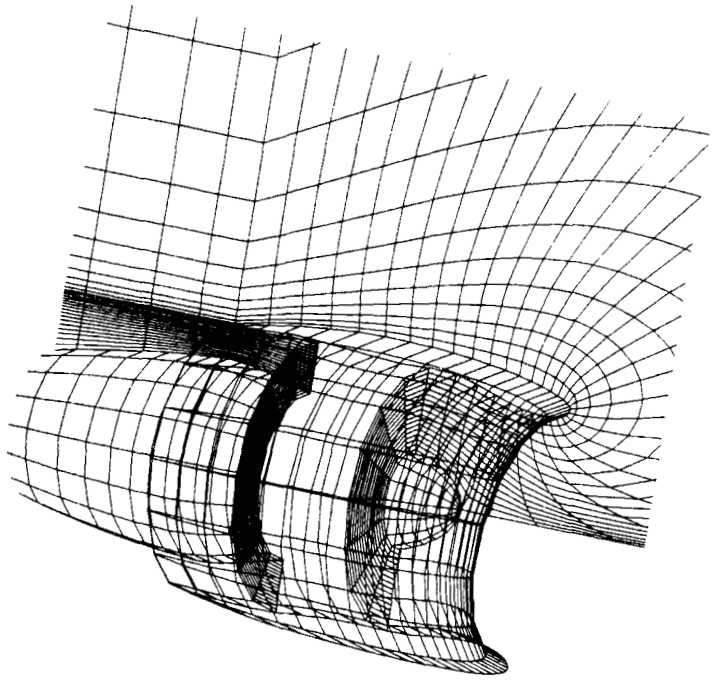

Figure 17. Computational Grid for Euler Powered Nacelle Code.

A588 has proven to be highly accurate in the calculation of the flow over isolated nacelles. Figure 18 shows the comparison of computed results with experimental data on a axisymmetric nacelle. The test data were acquired on a swept strut-mounted flow-through nacelle over a Mach number range from 0.70 to 0.925. A fixed mass flow ratio based on an experimental internal inlet pressure was specified for all the cases. The results shown in Figure 18 are typical of the very good agreement with test data that was obtained across the Mach number range.

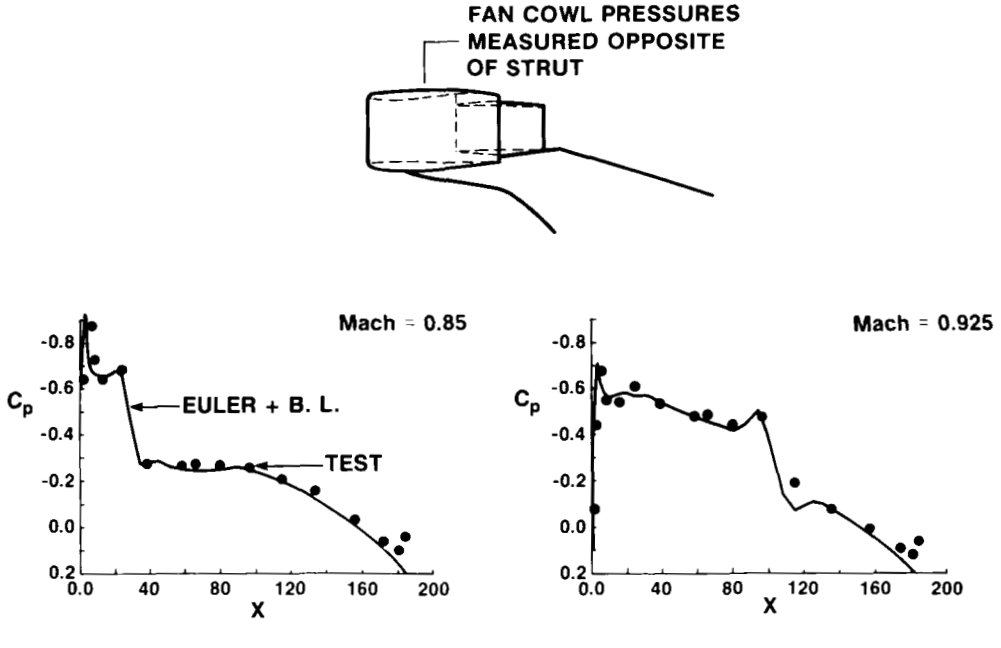

Figure 18. Comparison With Fan Cowl Pressures.

The second example of A588 analysis features a turbofan nacelle with a 5-deg drooped inlet. A comparison of the computed results and test data is shown in Figure 19. The test data were acquired on a swept strut-mounted flow-through nacelle. The inlet mass flow ratio for the test was calibrated in a model altitude test chamber. The test data were taken on the keel line, the right and left sides, and at about 30-deg right and left off the crown line along the side of the mounting pylon. The computations were done for the test Mach number, angle of attack, and inlet mass flow ratio. The discrepancy near the crown line can be attributed to a lack of modeling the mounting strut that was not included in this particular calculation. Note the variation of suction peak and shock strength around the circumference of the nacelle. The lack of perfect agreement with the suction peak around the circumference of the inlet might be attributed to a slight mismatch with the actual test angle of attack and mass flow, and to the geometric tolerances between the geometry tested and that used in the analysis. Note that the test data do not show perfect left/right symmetry. However, the overall agreement is good.

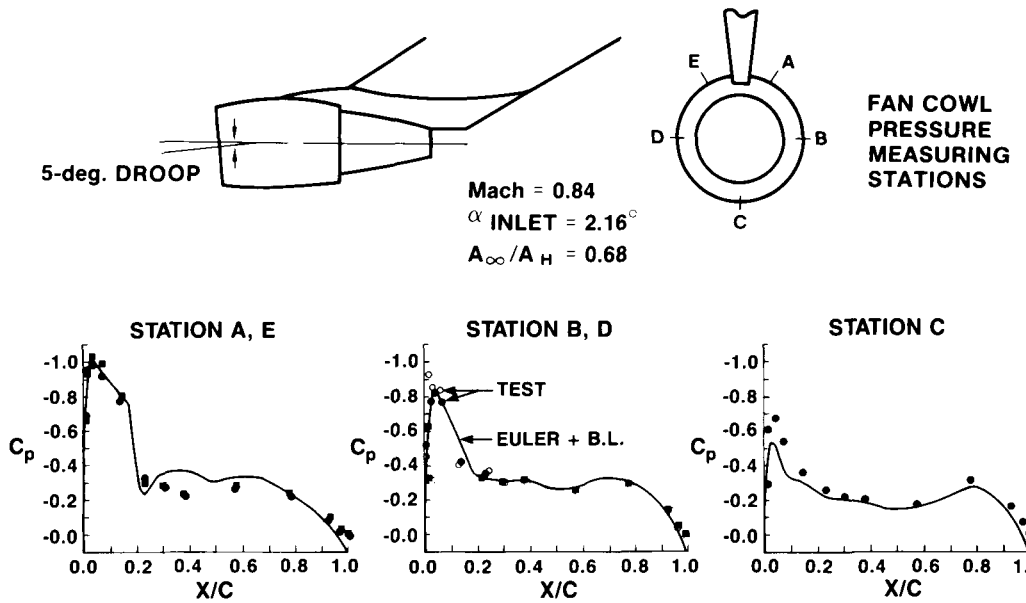

Figure 19. Fan Cowl Pressures on Nacelle at Angle of Attack.

A588 has demonstrated the ability to accurately predict nacelle drag, where drag is defined from the aerodynamicists view as the external fan cowl drag. The internal drag is accounted for by the propulsion engineer in the engine thrust-drag bookkeeping. For wind tunnel testing, the internal drag is determined in a model altitude test chamber. A comparison of A588 results (plus a handbook profile drag estimate for the mounting strut) with experimental data is shown in Figure 20. Note the excellent agreement for both drag level and drag rise. These types of comparisons have been made for a variety of nacelles. As long as the flow remains attached in the computational analysis, then usually any disagreement between test and A588 indicates a problem with the test data.

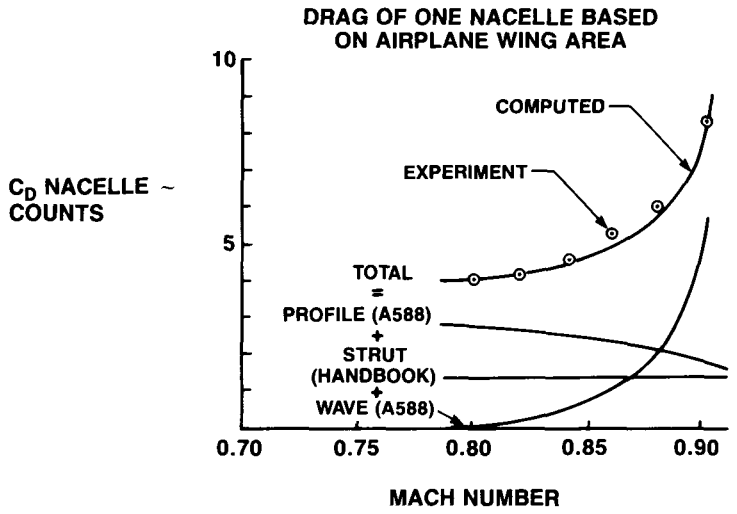

Figure 20. Fan Cowl Drag Rise—Comparison With Experiment.

Other useful production analysis codes include: P318, an axisymmetric full-potential code with boundary layer (ref 18); P467 axisymmetric geometry, three-dimensional full potential with the same three-dimensional boundary layer code used in A488; and P582, a three-dimensional full-potential cartesian grid code that can handle completely general geometries (ref 19). P318 is used because of its low cost to develop the initial lines of a nacelle, treating the crown, keel, and sides as separate geometry. The more complete A588 is then used to refine and validate the design. P582 has been used to analyze difficult geometries such as a tractor turboprop with an offset chin inlet (ref 20).

EXPERT USER TOOLS

Expert user tools or codes either have not yet matured enough in their development, or require skills generally not available outside the research environment for successful use. This category includes a series of codes based on the Euler formulation, specifically Jameson's FLO57 technology. The Euler formulation is of particular interest when dealing with rotational flows, i.e., flows of varying total temperature, total pressure, and swirl, and with flows in which trailing wakes from one surface may interact with another surface. These codes have been extended to handle complex transport type airplane configurations, illustrated in Figures 21 and 22, featuring wing, body, vertical, and horizontal tails, body-mounted engine nacelle and pylon, and propfan simulator disk, or wing mounted nacelle tractor propfans (refs 21 to 25). The complexity of the grid generation for these configurations currently precludes routine "production" use of this capability by users outside the research community. Another use of these Euler based codes has been in the analysis of a detailed propfan nacelle including pylon and simulator disk, illustrated in Figure 23, and engine exhaust flows (refs 26 and 27).

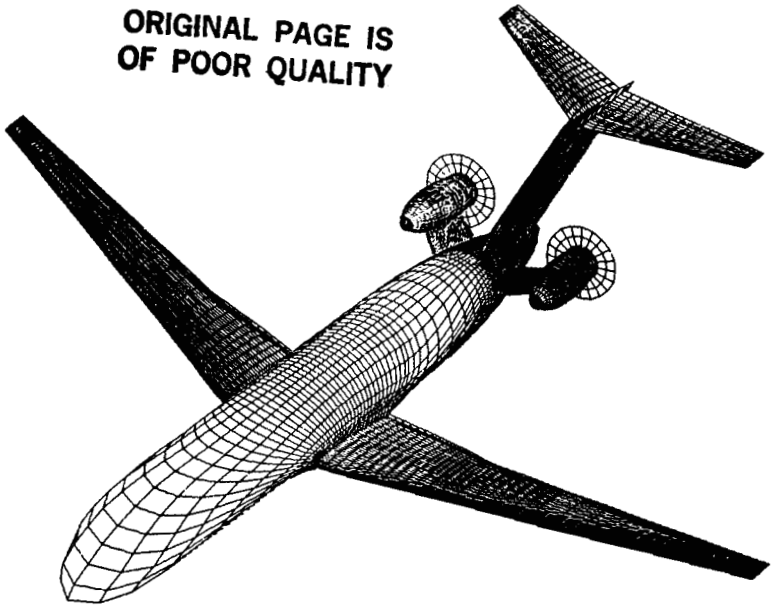

Figure 21. Surface Grid on Advanced Propfan Transport.

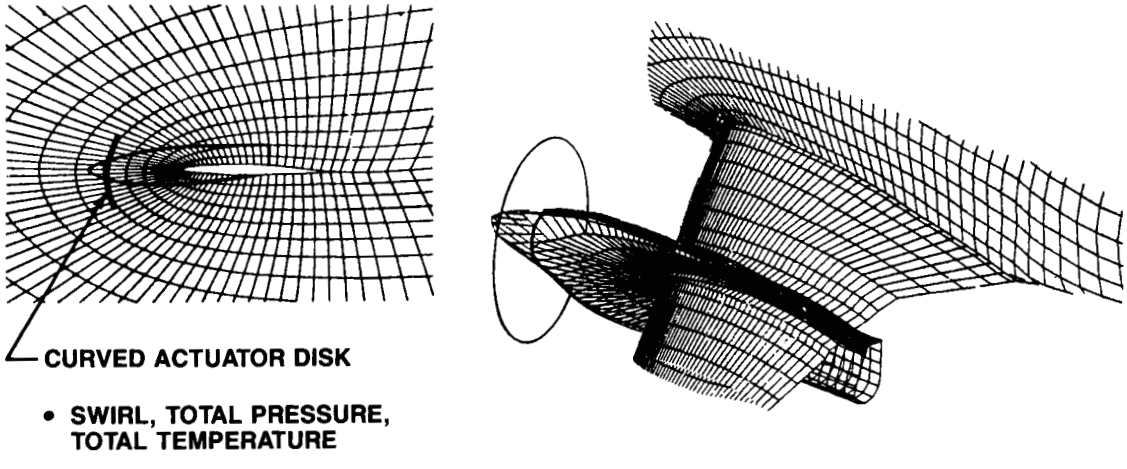

Figure 22. Grid for Wing-Mounted Tractor Propfan.

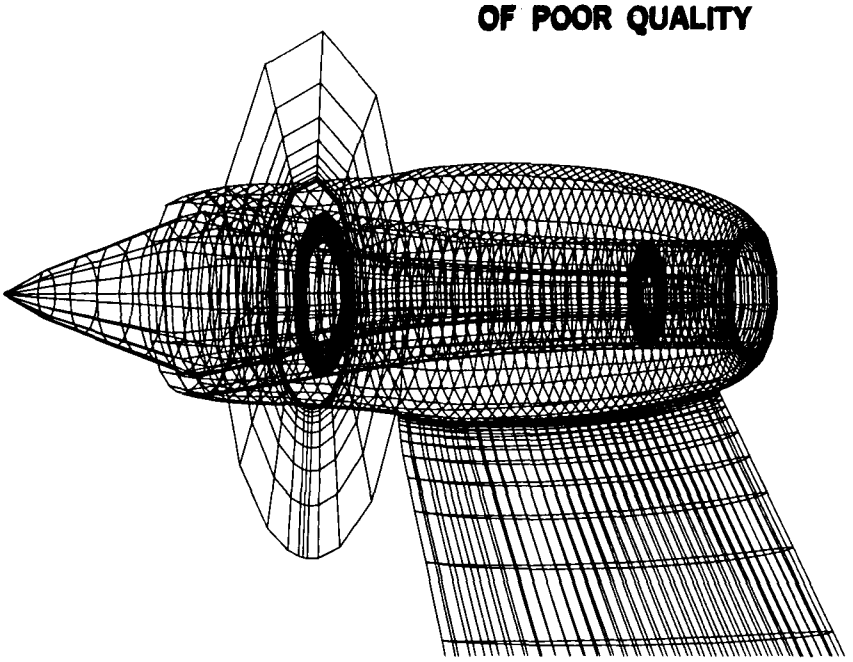

Figure 23. Grid for UDF Nacelle and Strut.

The basic solution technology for the unsteady Euler equations originated from Jameson's finite volume approach (FLO57) (ref 17) used in A588. In order to deal with much larger problems and more complex flows associated with complex aircraft configurations, considerable enhancements and improvements have been made to the basic technology which include; four- or five-stage Runge-Kutta time integration, a new dissipation model based on spectral radius scaling, a multigrid technique together with successive mesh refinement to speed up the convergence, and a multiblock treatment. The basic idea of the multiblock approach is to divide the complete flowfield into several blocks, such that the flowfield data within each block can fit in the existing central memory of a supercomputer. The complete flowfield data are stored on a solid state disk (SSD), and the computation is done in a block-by-block manner through the use of highly efficient input/output (I/O) data management. The flowfield in each block is advanced in time through one multigrid cycle. Within each grid level, a four or five-stage, explicit, Runge-Kutta time integration scheme, together with an implicit smoothing method, is used to update the flow variables to a new time level. The updated flowfield data are then moved to the SSD before another block of flowfield data is transferred to the central memory. The blocks of boundary data that are needed for the adjacent blocks in the flux and dissipation term calculations are saved in different locations on the SSD, so that they can be fetched during the calculation process. At the present time, the program is written such that the flowfield can be divided into an arbitrary number of blocks in both normal and spanwise directions to handle large problems. However, the general strategy is to keep the number of blocks to a minimum, for efficient vector processing. A solution for a wing-body-tail configuration (ref 23) is shown in Figures 24 and 25. The multiblock approach allows sufficient grid density to adequately capture the complex shock pattern on the wing, and the detailed interaction between the vertical and horizontal tail surfaces on the aftbody as indicated by the pressure contours shown in Figure 24. A comparison of the inviscid solution with experimental data shown in Figure 25, shows reasonable agreement.

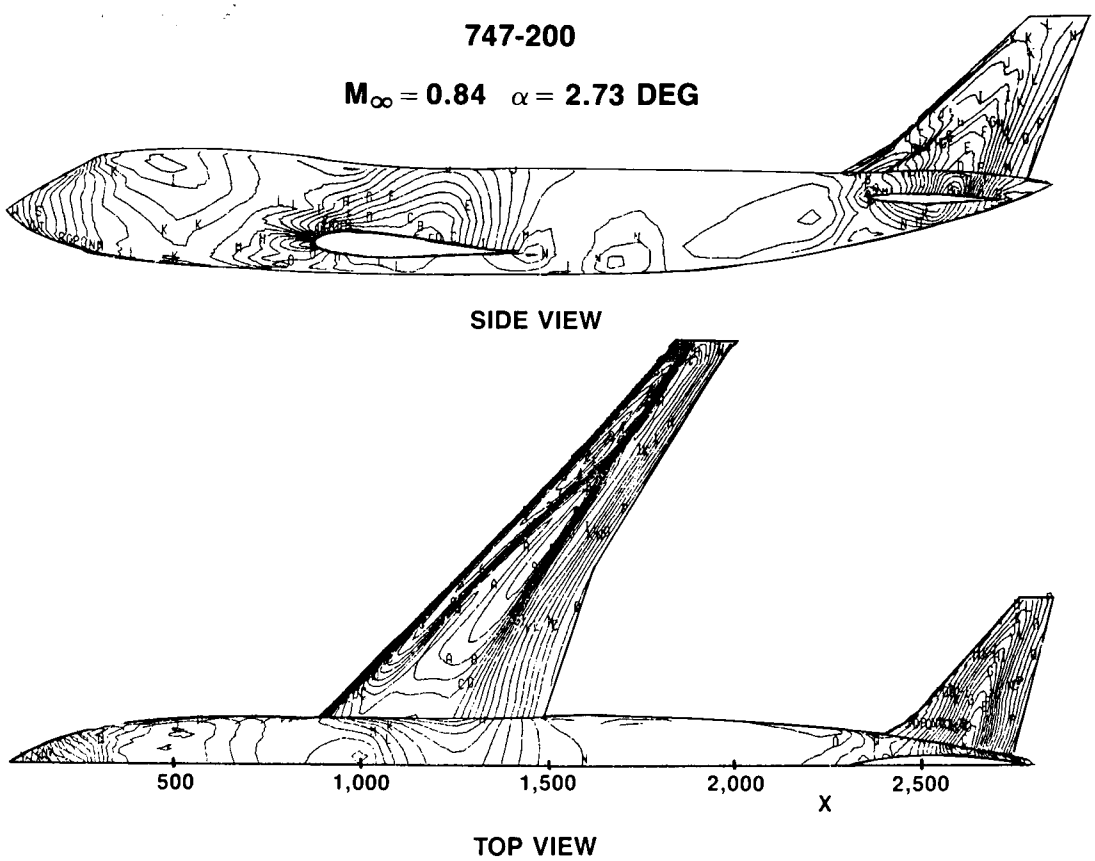

Figure 24. Surface Isobars for A 747-200 Configuration.

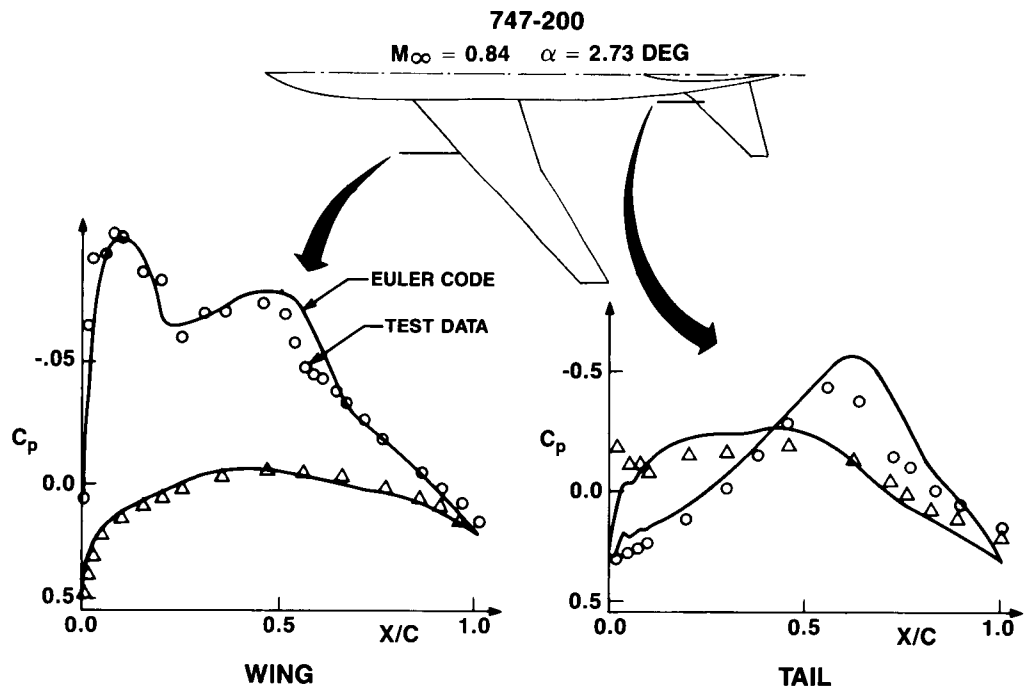

Figure 25. Comparison With Wing and Tail Pressure Distributions.

For a configuration with a propfan actuator disk, the program logic is greatly simplified if the propfan region including the propeller disk is kept in one block, such that the various boundary conditions on the propeller disk and exhaust plume can be implemented within a specified block. The propeller power loading is simulated by an actuator disk where the total pressure, total temperature, and swirl distributions are prescribed (ref 21). Another way of simulating propeller power effects is to prescribe the thrust, normal force, and sideforce in the propeller disk plane. The flow variables downstream of the disk are related to their corresponding upstream values through the use of continuity, momentum, and energy equations. The major advantages of this method are that the effects of angle of attack as well as the influence of side flow can easily be simulated through the input of normal and side force distributions along the propeller disk (ref 26).

A major application of this technology has been to the analysis of an advanced propfan powered aircraft, previously shown in Figure 21. A primary concern for a configuration with aft-mounted propfan engines is the power-induced interference effects on the aircraft's aerodynamics. While many of these characteristics can be investigated in the wind tunnel with powered propfan simulators, some conditions cannot. Small and powerful enough propfan simulators for testing at transonic conditions on a full model in yaw were not available to us at the time of this analysis. The asymmetric effects of a failed engine at cruise could only be investigated by computational methods. (This may still be the case today.) A full configuration analysis at both high and low speeds, and at yaw with various combinations of thrust on the right and left side engines was carried out to look at these issues. A grid of approximately 600,000 cells was used (ref 24). The CPU time on a CRAY X-MP for a solution was approximately two hours. The power induced effects at high speed on the pressure distributions on the vertical and horizontal tail surfaces are illustrated in Figures 26 and 27. For a low-speed, high-angle-of-attack case, the resulting moments and side force are shown in Figure 28. This type of information is very important to the stability and control engineer in estimating the handling characteristics of the aircraft.

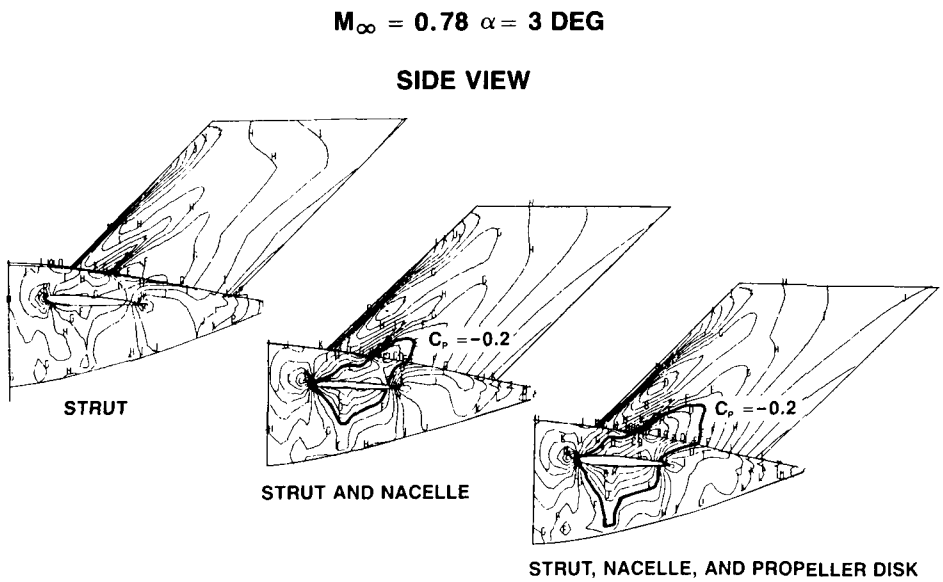

Figure 26. Effects of Propeller Power on Aftbody Isobars— Side View.

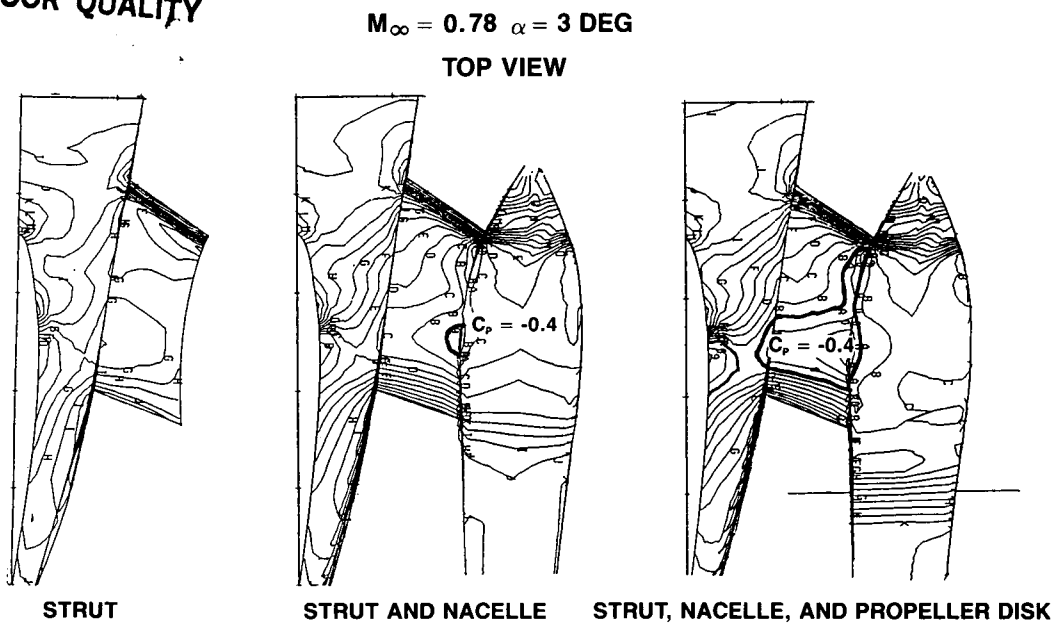

Figure 27. Effects of Propeller Power on Aftbody Isobars—Top View.

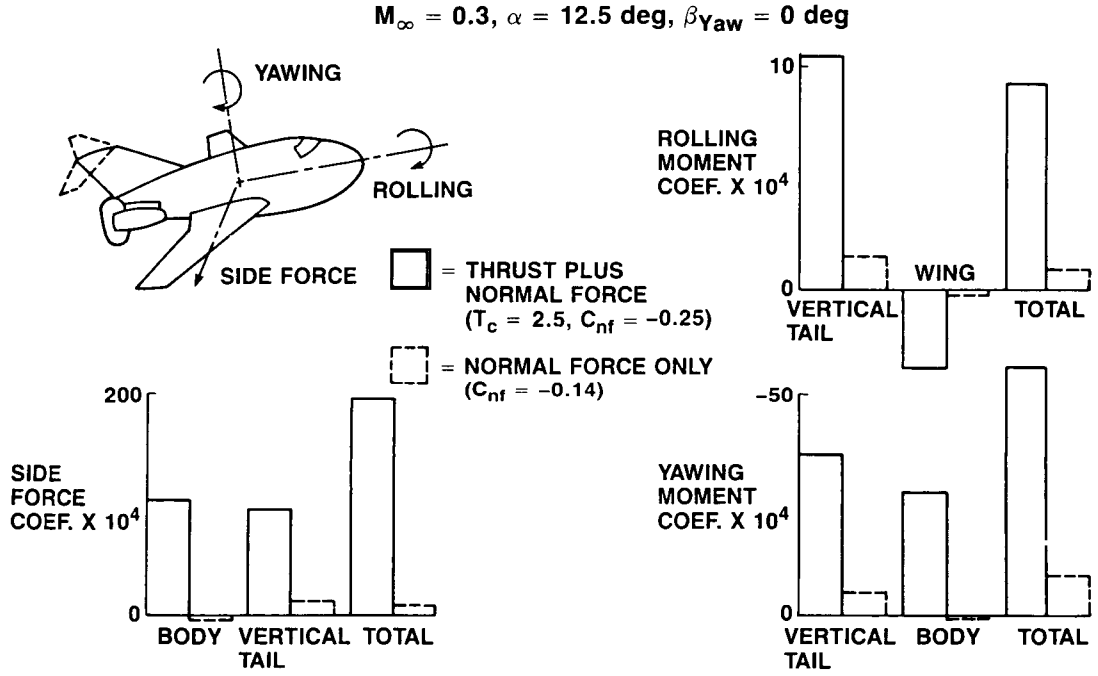

Figure 28. Effects of Asymmetric Thrust on Aircraft.

The Euler solver has also been incorporated into the boundary layer cycling package used in the A488 system previously described. In this implementation the boundary layer coupling can be applied to both wing and tail lifting surfaces. To improve the viscous coupling a contracting wake model has been added to the Euler solver (ref 25). This analysis package is being refined to include coupled solutions on full and partial chord winglet configurations.

The natural manner in which propulsion effects can be handled in the Euler formulation makes this the technology of choice for many problems. However, the level of expertise required to create the necessary surface-fitted grids will limit its use to a select few for the time being.

EMERGING TOOLS

Two essential characteristics of a valuable CFD tool are timeliness and the ability to handle complex "real world" geometry. Requirements for CFD analysis extend far beyond the analysis of simple wing-body configurations. The multiblock Euler approach shows a promising capability to analyze rather complex geometries, but it is questionable whether the necessary surface-fitted grid generation could be done in a timely fashion. As finer details of the geometry become of interest, the grid generation problems become more difficult. Work on unstructured grids (refs 28 and 29) may offer a solution to dealing with complex geometries. For now, the structured surface-fitted grid Euler tools will continue to be special purpose tools used by expert users. But what about a "production" tool for timely analysis of transonic flows about complex geometries for use by CFDers outside the research community? Such a tool is emerging; it is called TRANAIR.

TRANAIR (refs 30 and 31) employs a new approach for solving the full-potential equation about arbitrary configurations. One of the most important features of this approach is its compatibility, in terms of user-provided inputs regarding the configuration boundary, with the existing A502/PANAIR panel method. More than two dozen CFDers throughout the Boeing Company are familiar with setting up inputs (panel models) for A502/PANAIR. There is already an extensive array of geometry tools, i.e., AGPS (ref 1), available for creating the necessary panel models, and there are no inherent limitations on the complexity of geometry that can be described. The inputs for analysis of complex configurations with geometric details of greatly varying length scales can be prepared in a timely manner. This is in sharp contrast to codes that use structured surface-fitted grids.

TRANAIR eliminates the need for the surface-fitted grid by using rectangular grids superimposed on the paneled boundary configuration, as illustrated in Figure 29. The flow both inside and outside the configuration is considered (although in aerodynamic applications, the internal flow is fictitious). A rectangular grid

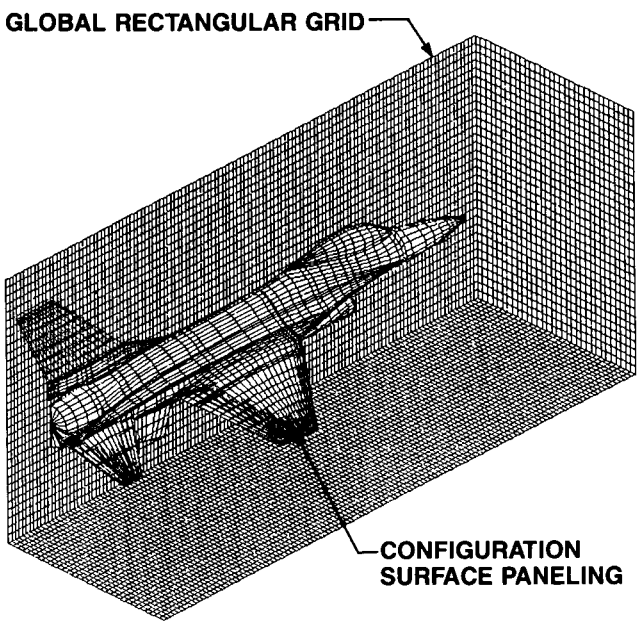

Figure 29. TRANAIR Grid Topology.

can always be superimposed on the configuration regardless of surface topology. The use of rectangular grids is not new. Rectangular grids have previously been used in small disturbance codes with linearized boundary conditions, and by Reyhner (ref 19), and others with "thick" geometries. What sets TRANAIR apart from previous codes is the use of finite element techniques to ensure that the discretization of the flowfield near the boundaries is flux conservative so that the conservation laws are imposed correctly and the global quantities of interest are predicted accurately, and now, the inclusion of automatic grid refinement near surface boundaries keyed to local panel density. The rectangular grid needs only to extend as far as the nonlinearities in the flowfield. The far field is handled by a discretized linear Prandtl-Glauert operator. The solution algorithm includes use of a Newton solver (nonlinear GMRES, ref 10) that uses the latest sparse matrix technology as a preconditioner. Future plans include the addition of hierarchical multigrid preconditioning.

The initial implementation of TRANAIR did not include the automatic grid refinement. Nevertheless, the computational results were very encouraging. The initial version of TRANAIR is well suited for compact objects such as fuselage forebody cabs, nacelles, etc. Figure 30 shows the paneling for a modern transport cab. The paneling is fine enough to resolve the crease line at the base of the windshield. A comparison of computed results from TRANAIR, A502/PANAIR, and experimental results is also shown in Figure 30. The TRANAIR results are in excellent agreement with the experimental data. As is typical of linear compressible flow theory, the A502/PANAIR results overpredict both the compression at the base of the windshield and the subsequent expansion.

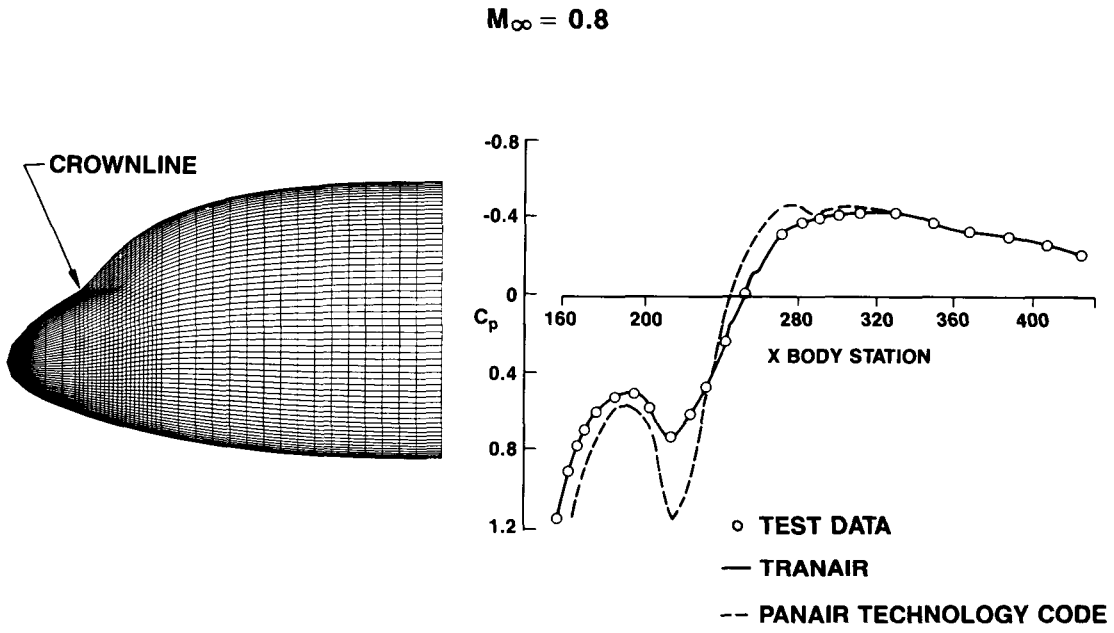

Figure 30. Transport Cab Analysis Test Theory Comparison.

A considerably more complex configuration that was analyzed with the initial TRANAIR was an F-16 fighter aircraft, shown in Figure 31. The configuration included the fuselage, canopy, wing, vertical and horizontal tail surfaces, and details of the inlet and exhaust regions. A total of 3000 panels were used to describe the surface geometry. A rectangular grid of 129 grid points in the x direction, 33 in the y direction, and 33 in the z direction was superimposed on the paneled configuration. The configuration was analyzed at both M = 0.6 and 0.9. In the subcritical solution, the residual error was reduced by 10 orders of magnitude in approximately 1350 CPU seconds on a CRAY X-MP. A comparison of the results for the Mach 0.6 case (not shown) with A502/PANAIR and experimental data on the wing showed excellent agreement except at the leading edge. For the supercritical Mach 0.9 case, the solution took 1500 CPU seconds to reduce the residual error by four orders of magnitude.

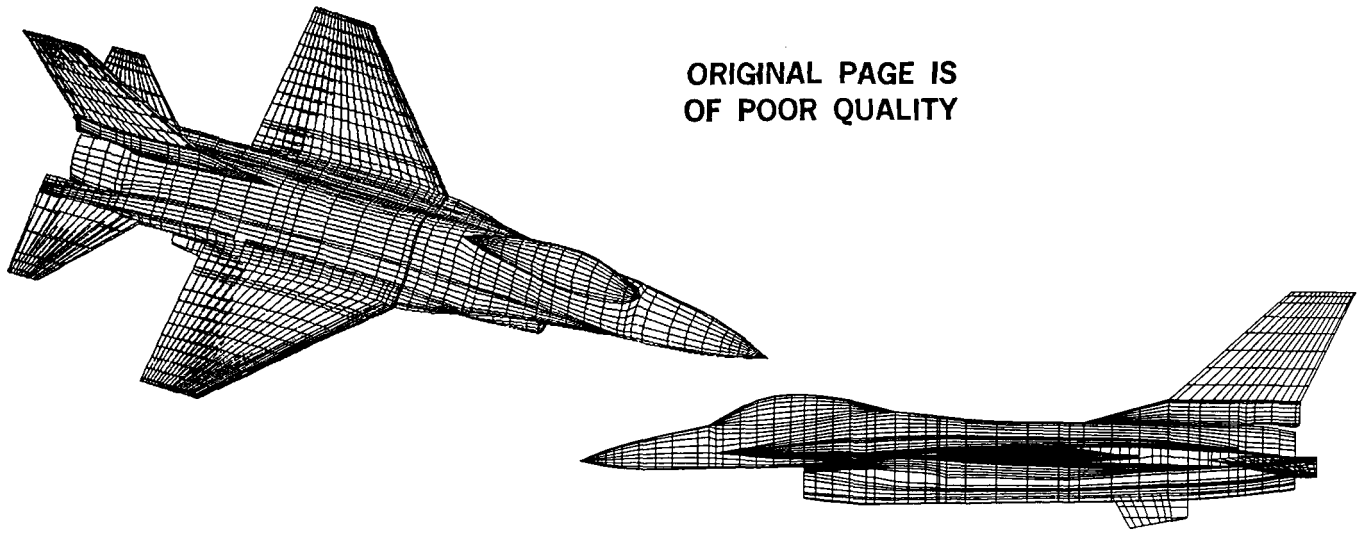

Figure 31. Surface Paneling for F-16 Fighter Aircraft.

A comparison of TRANAIR results for the Mach 0.90 analysis of the F-16 configuration with experimental data on the wing is shown in Figure 32. The agreement with experimental data is quite good except at the leading edge. The shock is well captured, albeit further aft than indicated by the experimental data. This is to be expected for an inviscid solution without viscous coupling. The discrepancy at the leading edge is easily understood when the coarseness of the global grid is taken into account (fig 33). The automatic grid refinement completely eliminates this shortcoming. Figure 34 shows the resulting grid after four levels of refinement. Note that the refinement takes place in three dimensional space. Each rectangular grid cell is divided into eight similar cells at each level of refinement. Figure 35 illustrates how the grid refinement ensures the resolution of detailed surface features. The user can specify the regions of space for refinement and the number of levels of refinement. The use of the automatic grid refinement allows use of a much sparser global grid with grid enrichment only where it is needed. As a consequence, the total number of grid cells can be kept to a reasonable number. At this time (December 1987) solutions for the F-16 with the grid refinement were not yet available. Additional TRANAIR F-16 results from the initial version without grid refinement can be found in reference 32.

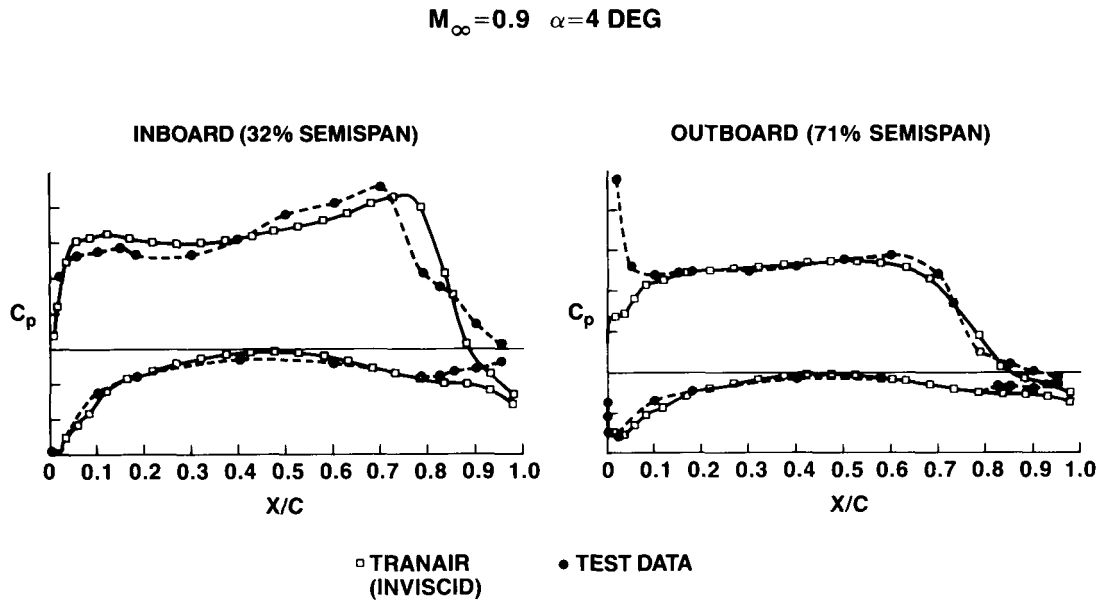

Figure 32. Comparison of Wing Surface Pressures on F-16 Configuration.

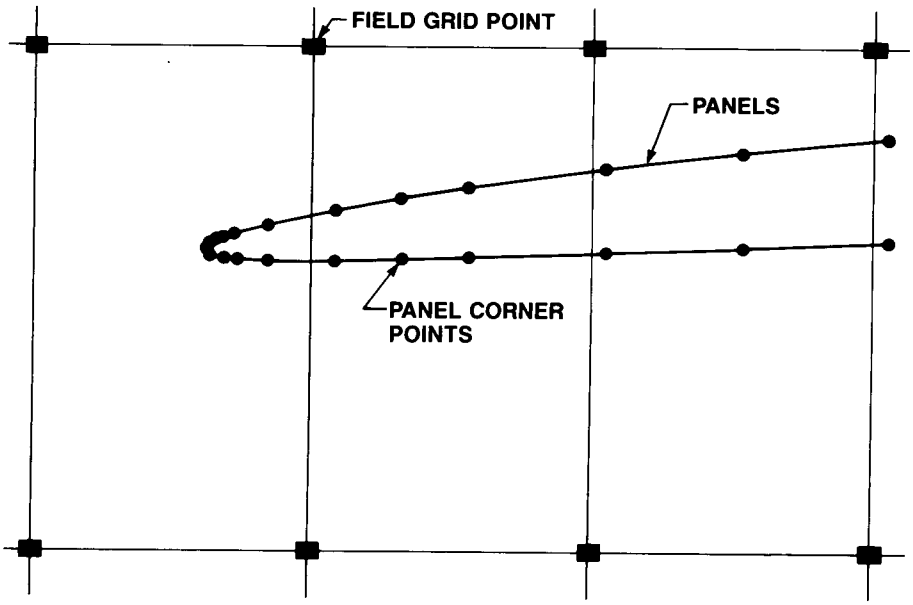

Figure 33. Relative Sizes of the Grid Cells and Surface Panels.

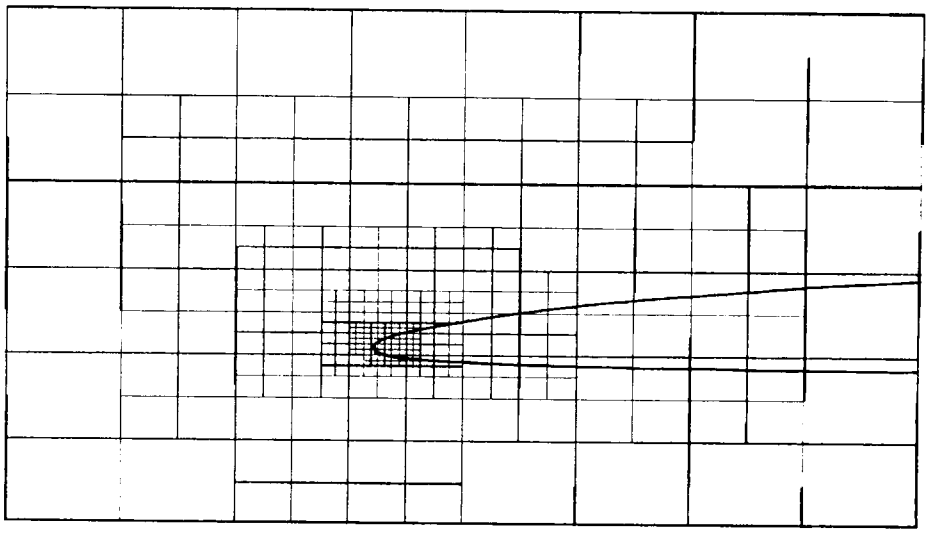

Figure 34. TRANAIR Automatic Grid Refinement Along Wing Leading Edge.

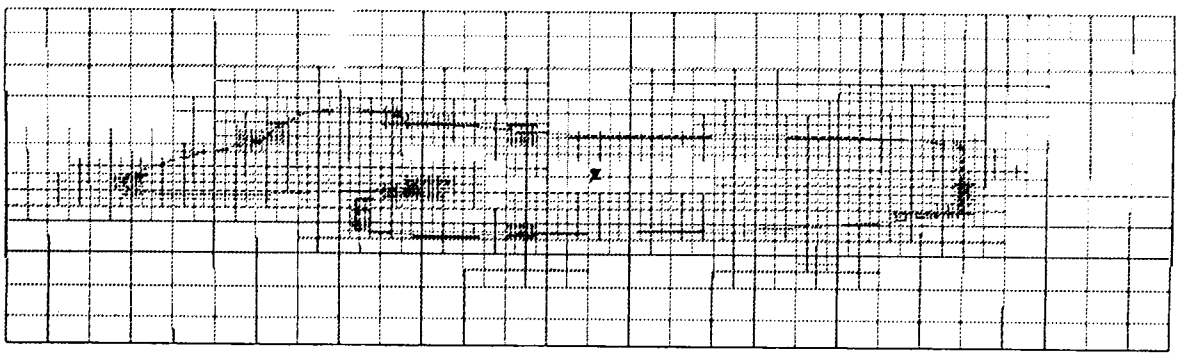

Figure 35. TRANAIR Automatic Grid Refinement on Fuselage—BBL = 20.

TRANAIR with grid refinement is scheduled to become available as a "production" code in 1988. Early indications are that subcritical TRANAIR solutions will be considerably cheaper than A502/PANAIR solutions for large cases, so we may see TRANAIR replacing that code. It is expected that automatic flowfield adaptive grid refinement will also become available in 1988 that will be very beneficial for supercritical solutions. Other anticipated improvements include a continued refinement of the algorithm to improve convergence rate, incorporation of the Hafez correction (ref 33) at the shock, possible wake capturing, and investigation of extending the method to the Euler equations. Plans are also being considered to incorporate some kind of viscous coupling similar to what is currently found in the A488 system and extending the code to the supersonic regime.

FUTURE CHALLENGES

One of the hottest CFD research fields today is in Navier-Stokes solvers. Many problems, particularly very high speed flows, and flows with significant separation, require the physical representation of the Navier-Stokes equations. But where should Navier-Stokes fit in for transonic analysis of transport type configurations? Limited use of Navier-Stokes has been made in a zonal approach to deal with jet exhaust interactions (refs 7 and 34), and with open cavities (ref 35). More recently, significant progress has been made by others in the application of Navier-Stokes to complete transport wing-body type configurations (refs 36 and 37), and to a fighter type configuration (ref 38). However, in industry, one does not replace a proven tool by a more expensive higher technology tool unless it offers a clear benefit.

The Navier-Stokes applications shown to date are at least one or two orders of magnitude more expensive than the inviscid/coupled viscous A488 solutions. For attached flow conditions we have yet to see evidence that the current Navier-Stokes solutions are more accurate. In fact, the A488 solutions may be the more accurate because of the significantly higher grid density used by the finite difference three-dimensional boundary layer solver, and empirical modeling of the shock-boundary layer interaction zone. When the Navier-Stokes solvers exceed the accuracy of the coupled A488 system there will still be the question of cost. As previously mentioned, A488 sees very heavy usage. During the last few years the number of A488 accesses throughout the Boeing Company have averaged over 2000 times a year. This number includes runs that failed, restarts for additional iterations, and just grid generation runs. That still leaves on the order of a 1000 complete analysis runs a year. An order of magnitude cost increase for this volume of analysis is not tolerable. In some wing design exercises, a very short time span is available for designing a wing for a wind tunnel entry. During these periods, quick turnaround is needed which is not practical with methods taking hours of CPU time.

At flight conditions resulting in some flow separation, the coupled inviscid/coupled viscous boundary layer codes will generally fail to converge to a useful solution. For these conditions Navier-Stokes may be able to provide flow information not accessible by lesser methods. However, experience has shown that the off-design handling characteristics of most interest are quite sensitive to the exact details of the flow separation phenomena. Details such as laminar to turbulent boundary layer transition location, and the effects of vortex generators, leading-edge snags, wing fences, vortilons, etc., can have very dramatic effects on the pitchup characteristics of an aircraft. When will Navier-Stokes solvers be able to account for these types of details?

The preceding discussion is not meant to discourage the researchers developing Navier-Stokes technology, but rather to point out some of the "real world" challenges that must be overcome for these methods to be used on a routine basis in industry. Many of the concerns related to determining off-design handling qualities are also present in low Reynolds wind tunnel testing and can only be fully addressed in flight at the present time. We will maintain an active vigilance on the progress being made in Navier-Stokes technology and will try to incorporate the appropriate methods into our CFD toolbox at the proper time.

CONCLUDING REMARKS

We have presented our current toolbox of CFD methods for three-dimensional transonic design and analysis and have illustrated their use through various applications. Production, expert user, and new emerg-

ing methods are all necessary parts of the toolbox. Just as a mechanic cannot work with a single wrench, we too need a mix of general purpose and special use tools. The competitive nature of the market place is forcing the Boeing Company to strive to a higher plane of excellence while reducing cost. In the aerodynamic design arena we are depending on CFD to provide the necessary leverage. However, to be of value CFD must be useful in a timely manner.

In early 1987, a critical wing design activity within Boeing reached an impass with regard to satisfying airplane performance requirements, wing structural requirements, and other practicalities necessary for a successful overall design. It was determined that an improvement in the transonic technology level of the wing could be used to satisfy all the necessary requirements. But in order to implement a new level of wing technology consistent with a tight program schedule, new designs would have to be assessed in the remainder of 1987 using available wind tunnel test windows. Two-dimensional analysis and design tools (refs 39 and 40) were used to develop a series of airfoils to investigate different pressure distributions consistent with a more aggressive design philosophy. After a confirming wind tunnel test, three wings for a wing-body configuration employing variations of the most promising design pressure distribution were designed using A488 and A555 in a time period of a little over a month. Each design, maintaining realistic structural and manufacturing constraints, required many cycles through A488 and A555, sometimes two or three cycles in a single day, to develop. These wings were a break from the previous evolution of Boeing designs, although similar designs had been tested in the early 1970s without much success.

The confirming wind tunnel test, conducted in the fall of 1987, included the three new wings and a previously designed baseline wing. The A488 analysis had predicted how the four wings would rank with respect to each other at the design cruise point. The wind tunnel test results confirmed the A488 predictions. The new wings were approximately 10% thicker than the baseline wing, but delivered the same drag level and drag divergence Mach capability. There were differences in details that the codes were not able to predict, so further refinement of the computational methods is still desirable. The wind tunnel was, of course, able to give information over a wider range of conditions than CFD. This endeavor was a success and was carried out in a very short period of time because of the skill of the responsible project engineers, and because the necessary tools were in place. No new code development or validation was necessary. However, several desirable enhancements to A488 and A555 were identified from the experience. They are being incorporated into the codes to further improve their usability and accuracy.

CFD is an integral part of the aerodynamic design process at Boeing. Together with the wind tunnel, designs are now being developed in a timely manner that was not previously possible. That is the role of CFD in industry.

ACKNOWLEDGMENTS

This paper is based in part on work conducted for the Boeing Independent Research and Development Program. The author would like to thank Dr. Allen W. Chen for his contributions to many of the examples shown. Thanks also goes to Drs. N. J. Yu and H. C. Chen for their Euler work contributions, Drs. F. T. Johnson, S. S. Sammant, and J. E. Bussoletti for their TRANAIR contributions, and to the various project engineers responsible for some of the examples presented.

REFERENCES

1. Snepp, D. K. and Pomeroy, R. C., "A Geometry System for Aerodynamic Design," AIAA Paper 87-2902, September 1987.

2. Moran, J., Tinoco, E. N., and Johnson, F. T., "User's Manual—Subsonic/Supersonic Advanced Panel Pilot Code," NASA CR-152047, 1978.

3. Derbyshire, T. and Sidwell, K. W., "PAN AIR Summary Document, (Version 1.0)," NASA CR-3250, 1982.

4. daCosta, A. L., "Application of Computational Aerodynamics Methods to the Design and Analysis of Transport Aircraft," ICAS Paper 78.B2-01, September 1978.

5. Yu, N. J., "Grid Generation and Transonic Flow Calculations for Three-Dimensional Configurations," AIAA Paper 80-1391, July 1981.

6. Yu, N. J., "Transonic Flow Simulations for Complex Configurations with Surface Fitted Grids," AIAA-81-1258, June 1981.

7. Tinoco, E. N. and Chen, A. W., "CFD Applications to Engine/Airframe Integration," Numerical Methods for Engine-Airframe Integration, Vol. 102 of Progress in Astronautics and Aeronautics, AIAA, 1986.

8. Caughey, D. A. and Jameson, A., "Recent Progress in Finite Volume Calculations for Wing-Fuselage Combinations," AIAA Paper 79-1513, 1979.

9. Yu, N. J. and Rubbert, P. E., "Acceleration Schemes for Transonic Potential Flow Calculations," AIAA Paper 80-0338, January 1980.

10. Wigton, L. B., Yu, N. J., and Young, D. P., "GMRES Acceleration of Computational Fluid Dynamics Codes," AIAA Paper 85-1494, June 1985.

11. McLean, J. D. and Randall, J. L., "Computer Program to Calculate Three-Dimensional Boundary Layer Flows over Wings with Wall Mass Transfer," NASA CR-3123, 1978.

12. McLean, J. D. and Matoi, T. K., "Shock/Boundary-Layer Interaction Model for Three-Dimensional Transonic Flow Calculations," Turbulent Shear Layer/Shock Wave Interactions IUTAM Symposium Palaiseau 1985, Springer, Berlin Heidelberg 1986.

13. Rozendaal, R. A., "Variable Sweep Transition Flight Experiment (VSTFE)-Parametric Pressure Distribution Boundary Layer Stability Study and Wing Glove Design Task," NASA CR-3992, June 1986.

14. Squire, H. B. and Young, A. D., "The Calculation of the Profile Drag of Aerofoils," Aeronautical Research Committee, Reports and Memoranda No. 1838, London, November 1937.

15. Boppe, C. W., "Aerodynamic Analysis for Aircraft with Nacelles, Pylons, and Winglets at Transonic Speeds," NASA CR-4066, April 1987.

16. Chen, H. C., Yu, N. J., Rubbert, P. E., and Jameson, A., "Flow Simulations for General Nacelle Configurations Using Euler Equations," AIAA Paper 83-0539, 1983.

17. Jameson, A., Schmidt, W., and Turkel, E., "Numerical Solutions of the Euler Equations by Finite Volume Methods Using Runge-Kutta Time-Stepping Schemes," AIAA Paper 81-1259, 1981.

18. Colehour, J. L., "Transonic Flow Analysis Using a Streamline Coordinate Transformation Procedure," AIAA Paper 73-0657, July 1973.

19. Reyhner, T. A., "Three-Dimensional Transonic Potential Flow About Complex Three-Dimensional Configurations," NASA CR-3814, July 1984.

20. Sokhey, J. S., "Three-Dimensional Transonic Flow Analysis of Turboprop Inlet and Nacelle Configurations," AIAA Paper 84-0193, January 1984.

21. Yu, N. J., Samant, S. S., and Rubbert, P. E., "Flow Predictions for Propfan Configurations Using Euler Equations," AIAA Paper 84-1645, June 1984.

22. Samant, S. S., and Yu, N. J., "Flow Prediction for Propfan Engine Installation Effects on Transport Aircraft at Transonic Speeds," NASA CR-3954, January 1986.

23. Yu, N. J., Kusunose, K., Chen, H. C., and Summerfield, D. M., "Flow Simulations for a Complex Airplane Configuration Using Euler Equations," AIAA Paper 87-0454, January 1987.

24. Kusunose, K, Marcum, D. L., Chen, H. C., and Yu, N. J., "Transonic Analysis for Complex Airplane Configurations," AIAA Paper 87-1196, June 1987.

25. Chen, H. C., Yu, N. J., Marcum, D. L., Kao, T. J., and Kusunose, K., "Coupled Euler/Boundary Layer Analysis of a Complete Aircraft with Viscous Modeling on the Lifting Surface," AIAA Paper 87-2614-CP, August 1987.

26. Yu, N. J., and H. C. Chen, "Flow Simulations for Nacelle-Propeller Configurations Using Euler Equations," AIAA Paper 84-2143, August 1984.

27. Chen, H. C., Kusunose, K., and Yu, N. J., "Flow Simulations for Detailed Nacelle-Exhaust Flow Using Euler Equations," AIAA Paper 85-5003, October 1985.

28. Jameson, A. and Baker, T. J., "Improvements to the Aircraft Euler Method," AIAA Paper 87-0452, January 1987.

29. Lohner, R., Morgan, K., and Peraire, J., "Improved Adaptive Refinement Strategies for the Finite Element Aerodynamic Configurations," AIAA Paper 86-0499, January 1986.

30. Rubbert, P. E., Bussoletti, J. E., Johnson, F. T., Sidwell, K. W., Rowe, W. S., Samant, S. S., SenGupta, G., Weatherill, W. H., Burkhart, R. H., Everson, B. L., Young, D. P., and Woo, A. C., "A New Approach to the Solution of the Boundary Value Problem Involving Complex Configurations," Symposium on Future Directions in Computational Mechanics, Anaheim, California, December 1986.

31. Samant, S. S., Bussoletti, J. E., Johnson, F. T., Burkhart, R. H., Everson, B. L., Melvin, R. G., and Young, D. P., "TRANAIR: A Computer Code for Transonic Analyses of Arbitrary Configurations," AIAA Paper 87-0034, January 1987.

32. Erickson, L. L., Madson, M. D., and Woo, A. C., "Application of the TRANAIR Full Potential Code to Complete Configurations," ICAS-86-1.3.5, 1986.

33. Hafez, M. M., Murman, E. M., and South, J. C., "Artificial Compressibility Methods for Numerical Solution of Transonic Full Potential Equations," AIAA Paper 78-1148, 1978.

34. Roberts, D. W., "Prediction of Subsonic Aircraft Flows with Jet Exhaust Interaction," Aerodynamics of Power Plant Installation, AGARD-CP-301, Paper 32, May 1981.

35. Om, D., "Navier-Stokes Simulation for Flow Past an Open Cavity," AIAA Paper 86-2638, October 1986.

36. Obayashi, S., Fujii, K., and Takanashi, S., "Toward the Navier-Stokes Analysis of Transport Aircraft Configurations," AIAA Paper 87-0428, January 1987.

37. Takanashi, S., Obayashi, S., Matsushima, K., and Fujii, K., "Numerical Simulation of Compressible Viscous Flows Around Practical Aircraft Configurations," AIAA Paper 87-2410CP, August 1987.

38. Flores, J., Reznick, S. G., Holst, T. L., and Gundy, K., "Navier-Stokes Solutions for a Fighter-Like Configuration," AIAA Paper 87-0032, January 1987.

39. Drela, M. and Giles, M. B., "Viscous-Inviscid Analysis of Transonic and Low Reynolds Number Airfoils," AIAA Paper 86-1786, June 1986.

40. Giles, M. B., and Drela, M., "A Two-Dimensional Transonic Aerodynamic Design Method," AIAA Paper 86-1793, June 1986.